



# 1 Biomass-burning derived particles from a wide variety of 2 fuels: Part 1: Properties of primary particles

3 Crystal D. McClure<sup>1</sup>, Christopher Y. Lim<sup>2,%</sup>, David H. Hagan<sup>2</sup>, Jesse H. Kroll<sup>2</sup>, Christopher D.  
4 Cappa<sup>1,3,\*</sup>

5 <sup>1</sup>Department of Civil and Environmental Engineering, University of California, Davis, CA 95616

6 <sup>2</sup>Department of Civil and Environmental Engineering, Massachusetts Institute of Technology,  
7 Cambridge, MA, USA

8 <sup>3</sup>Atmospheric Sciences Graduate Group, University of California, Davis, CA, USA 95616

9 <sup>%</sup> Now at Department of Chemistry, University of Toronto, Ontario, Canada

10 \* To whom correspondence should be addressed: cdcappa@ucdavis.edu

## 11 ABSTRACT

12 Relationships between various optical, physical, and chemical properties of biomass  
13 combustion derived particles are characterized for particles produced from a wide range of fuels  
14 and burn conditions. The modified combustion efficiency (MCE), commonly used to parameterize  
15 biomass particle emissions and properties, is shown to generally have weak predictive capabilities,  
16 especially for more efficient combustion conditions. There is, however, a strong relationship  
17 between many intensive optical properties (e.g. single scatter albedo, Ångstrom absorption  
18 exponent, mass absorption efficiency) and the organic aerosol-to-black carbon ([OA]/[BC]) mass  
19 ratio over a wider range than previously considered (0.3 to 10<sup>5</sup>). The properties of brown carbon  
20 (BrC, i.e. light absorbing organic carbon) also vary with [OA]/[BC]. The contribution of coating-  
21 induced enhancements (i.e. “lensing” effects) to absorption by black carbon are shown to be  
22 negligible for all conditions. The BC-OA mixing state varies strongly with [OA]/[BC]; the fraction  
23 of OA that is internally mixed with BC decreases with [OA]/[BC] while the relative amount of  
24 OA coated on BC increases. In contrast, there is little relationship between many OA bulk chemical  
25 properties and [OA]/[BC], with the O:C and H:C atomic ratios and the relative abundance of a key  
26 marker ion ( $m/z = 60$ , linked to levoglucosan) all showing no dependence on [OA]/[BC]. In  
27 contrast, both the organic nitrate fraction of OA and the OA volatility do depend on the [OA]/[BC].  
28 Neither the total particle or BC-specific size distributions exhibit any clear dependence on the burn  
29 conditions or [OA]/[BC], although there is perhaps a dependence on fuel type. Overall, our results  
30 expand on existing knowledge to contribute new understanding of the properties of particles  
31 emitted from biomass combustion.



## 32 1 Introduction

33 While it is understood that both open and controlled biomass combustion are major sources of  
34 particles to the atmosphere (Andreae and Merlet, 2001), questions remain regarding the properties  
35 of the emitted particles, their relationship with combustion conditions and fuel type, and their  
36 atmospheric evolution. Particles emitted from biomass combustion impact the global radiation  
37 budget and contribute to poor air quality in impacted regions. The emitted primary particles are  
38 primarily composed of organic aerosol (OA) and black carbon (BC), in varying amounts, with  
39 trace inorganic species (Reid et al., 2005;McMeeking et al., 2009;Levin et al., 2010). Particle  
40 intensive properties are often compared against the modified combustion efficiency (MCE  $\sim$   
41  $\Delta[\text{CO}_2]/(\Delta[\text{CO}] + \Delta[\text{CO}_2])$ ), which provides a measure of the combustion efficiency of a burn. For  
42 example, various particle properties show some relationship with MCE, but often these  
43 relationships are weak, especially for more efficient combustion (higher MCE, corresponding  
44 typically to flaming conditions) (McMeeking et al., 2009;Liu et al., 2013;McMeeking et al., 2014).  
45 Understanding the diversity in the chemical, physical, and optical properties of the emitted  
46 particles is important for establishing the fire- or region-specific emissions and subsequent  
47 impacts.

48 The emitted OA from biomass combustion is somewhat light absorbing (Kirchstetter et al.,  
49 2004). Absorbing OA is commonly referred to as brown carbon (BrC), with properties that appear  
50 to depend on the fuel and combustion conditions (Saleh et al., 2014;Laskin et al., 2018), which  
51 affect particle organic composition (Jen et al., 2019). However, the properties of primary BrC  
52 absorption and, especially, understanding of the relationships between BrC absorption and other  
53 particle properties and burn conditions is only beginning to be unraveled. Additionally, it is  
54 established from theory and laboratory experiments that non-absorbing coatings on black carbon  
55 and other strongly absorbing particles can enhance the absorption (commonly referred to as the  
56 “lensing” effect but more accurately termed here the coating-induced enhancement) (Fuller et al.,  
57 1999;Bond et al., 2006;Lack et al., 2009;Shiraiwa et al., 2010;Cappa et al., 2012). Yet, the extent  
58 to which coating-induced enhancements impact absorption by ambient particles or for mixed-  
59 component particles from complex sources, such as biomass burning, remains contentious (Cappa  
60 et al., 2012;Healy et al., 2015;Liu et al., 2015;Peng et al., 2016;Liu et al., 2017).



61 Here, we expand on current understanding of the relationships between various primary  
62 particle properties and burn conditions by analyzing measurements of primary biomass burning  
63 particles produced from combustion of a variety of fuel types, many of particular relevance to the  
64 western U.S.. We demonstrate that various optical properties exhibit a strong relationship with the  
65 [OA]/[BC] mass ratio, much stronger than their relationship with the MCE. We use the  
66 measurements to quantify the individual contributions of BC, BrC and from internal mixing of BC  
67 to the observed light absorption, and examine the variability in the properties of BrC specifically.  
68 We uniquely characterize the mixing state of BC and OA, and how mixing state vary between  
69 individual burns and depend on the mean properties of the emitted particles. We characterize the  
70 variability of OA-specific properties, including OA volatility, bulk chemical composition  
71 (characterized by the O:C and H:C atomic ratio, and the presence of key marker ions), and,  
72 uniquely, the relative abundance of organic nitrate species. We also examine the variability in the  
73 emitted particle size distribution, both for the total particles and for the BC particles specifically.  
74 Some of our analysis serves to support and extend previously determined relationships by  
75 considering a wider range of conditions, while other aspects are unique to this study. These  
76 observations provide a foundation for understanding and interpretation of experiments on the  
77 influence of photochemical aging on biomass particle properties, discussed in a related paper (Lim  
78 et al., 2019).

## 79 **2 Methods**

80 All experiments were conducted during the Fire Influence on Regional to Global Environments  
81 Experiment (FIREX) lab study, which took place at the Missoula Fire Sciences Lab in Missoula,  
82 MT, USA during November, 2016. Numerous types of biomass were combusted in a large  
83 chamber (12 x 12 x 19 m) and the smoke sampled to provide information on the physical, chemical,  
84 and optical properties of the resulting smoke (i.e., particulate and gas emissions). The general fuels  
85 types combusted included (exclusively or in combination): duff, dung, excelsior, straw, litter,  
86 untreated lumber, rotten debris, woody debris, shrub, herbaceous, and canopy biomass. A complete  
87 list of fuels and types is provided in **Table S1**, with further details available on the U.S. National  
88 Oceanic and Atmospheric Administration (NOAA) data archive  
89 (<https://esrl.noaa.gov/csd/projects/firex/>). All data used in this publication are also available on the  
90 NOAA archive, with the processed data summarized in complementary data repository (Cappa et  
91 al., 2019a).



92 Both “room” and “stack” burns were conducted, although here we include results only from  
93 stack burns. During stack burns, the smoke was mixed with background room air and funneled up  
94 a large cylindrical stack (2 m dia. x 15 m height) where it was sampled into a high-flow transfer  
95 line at ca. 0.27 m<sup>3</sup>/s. This flow rate corresponded to sampling approximately 10% of the stack  
96 flow. Smoke was transferred to an adjacent room via the high-flow transfer line (residence time  
97 ca. 2 s) where it was sub-sampled through a PM<sub>2.5</sub> cyclone and injected into a 0.25 m<sup>3</sup> Teflon  
98 photochemical reaction chamber (the mini chamber). Details on the construction and operation of  
99 the mini chamber can be found in (Lim et al., 2019). Here, we focus exclusively on the properties  
100 of particles sampled prior to initiation of photochemical oxidation; results of the photochemical  
101 oxidation experiments are discussed in a series of papers (Coggon et al., 2019; Lim et al., 2019).  
102 In brief, prior to each burn, the chamber was flushed with clean air with a relative humidity (RH)  
103 of approximately 40%. To fill the chamber, smoke was sub-sampled from the high-flow inlet and  
104 injected across the entire burn (typically lasting for 10-20 minutes) or until the chamber  
105 concentration reached a maximum. A suite of instruments sampled from the mini chamber at a  
106 flow rate of approximately 6 lpm. This flow rate varied from burn to burn due to the exact suite of  
107 instruments sampling. Clean makeup air was being injected simultaneously from a zero air  
108 generator to equal the air being sampled out of the chamber. The sampled smoke was diluted by a  
109 factor of ca. seven relative to the air in the high-flow inlet. Subsequent dilution after filling was  
110 characterized by the decay of acetonitrile (ACN). Properties of the primary particles are averaged  
111 over the 5-10 minute period after filling but before the initiation of photochemistry.

112 Particle-phase instrumentation sampled alternately every two minutes through a  
113 thermodenuded or ambient sample line. The thermodenuder was operated at 300 °C with a  
114 residence time of approximately 5 s and volatilized semi-volatile components, including those that  
115 are internally mixed with BC. The ambient line was lined with a charcoal cloth that removed excess  
116 gases (such as VOCs, NO<sub>x</sub>, and O<sub>3</sub>) that could interfere with particle-phase measurements.  
117 Comparison of thermodenuded versus ambient particles allowed for the investigation of coating  
118 amount and volatility. The gas-phase composition in the mini chamber was similar to that sampled  
119 directly from the fire (Koss et al., 2018; Lim et al., 2019). Particle phase instrumentation included:  
120 a multi-wavelength cavity-ringdown-photoacoustic absorption spectrometer (CRD-PAS) and a  
121 photoacoustic absorption spectrometer (PASS-3) for characterization of light absorption and  
122 extinction coefficients at 405 nm, 532 nm, and 781 nm; a high resolution aerosol mass



123 spectrometer (HR-ToF-AMS) for characterization of non-refractory submicron particulate matter  
124 (NR-PM<sub>1</sub>) components (i.e. OA, NO<sub>3</sub>, SO<sub>4</sub>, NH<sub>4</sub>, Cl, K); a soot photometer AMS (SP-AMS) in  
125 laser-only mode for characterization of refractory BC and the NR-components that are internally  
126 mixed with BC; a single particle soot photometer (SP2) for characterization of refractory BC mass  
127 concentrations and size distributions; and a scanning electrical mobility sizer (SEMS) for  
128 measurement of particle mobility size distributions. Further details regarding instrument operation  
129 and calibration are provided in the Supplemental Material and in Lim et al. (2019).

130

### 131 **3 Results and Discussion**

#### 132 **3.1 Bulk optical property relationships**

133 Due to the wide variety of biomass fuels and types used during FIREX, there was a substantial  
134 diversity in the properties of primary particles produced. Previous studies have shown both the  
135 single scatter albedo (SSA) and wavelength-dependence of absorption (the absorption Angstrom  
136 exponent, AAE) depend on the modified combustion efficiency (MCE) (Liu et al.,  
137 2013;McMeeking et al., 2014;Pokhrel et al., 2017). The MCE is defined here as:

$$138 \quad MCE = \frac{[CO_2]}{[CO_2]+[CO]} \quad (1)$$

139 The SSA is defined as:

$$140 \quad SSA = \frac{b_{ext}-b_{abs}}{b_{ext}} \quad (2)$$

141 where  $b_{ext}$  is the wavelength-specific extinction coefficient and  $b_{abs}$  is the wavelength-specific  
142 absorption coefficient. The AAE is defined as:

$$143 \quad AAE = -\log\left(\frac{b_{abs,\lambda_1}}{b_{abs,\lambda_2}}\right) / \log\left(\frac{\lambda_1}{\lambda_2}\right) \quad (3)$$

144 where  $\lambda_1$  and  $\lambda_2$  indicate two different wavelengths, here 405 nm and 532 nm. The MCE  
145 characterizes the overall combustion efficiency, with values closer to unity indicating more  
146 complete combustion. In general, higher MCE correspond to more flaming combustion conditions  
147 while smaller MCE correspond to more smoldering conditions. We find a similar relationship  
148 between SSA<sub>405nm</sub>, AAE, and [OA]/[BC] with MCE as previous studies (**Figure 1**) (McMeeking



149 et al., 2009;Liu et al., 2013;McMeeking et al., 2014;Pokhrel et al., 2017). Specifically, the  
150  $SSA_{405\text{nm}}$  is relatively constant and near unity for  $MCE < \sim 0.9$ , but above this value exhibits a  
151 rapid decline, albeit with a substantial amount of scatter (**Figure 1a**). The AAE is also relatively  
152 constant when  $MCE < 0.9$ , with very large values ( $AAE \sim 8$ ). There is a rapid, scattered decrease  
153 in the AAE as MCE increases further (**Figure 1b**). The relationship between  $[OA]/[BC]$  and MCE  
154 is similar, with values generally decreasing as MCE increases but a large amount of scatter (**Figure**  
155 **1d**). There is also a general relationship between the mass absorption coefficient referenced to BC  
156 ( $MAC_{BC}$ ) at 405 nm and the MCE, but with similar scatter as the other properties (**Figure 1c**). The  
157  $MAC_{BC}$  is defined as:

$$158 \quad MAC_{BC} = b_{abs}/[BC] \quad (4)$$

159 The  $MAC_{BC,405\text{nm}}$  includes contributions from absorption by BC, BrC, and from coating-induced  
160 enhancement of BC absorption. These results, along with the literature, indicate that MCE can  
161 provide guidance as to the general magnitude of these particle properties, but that the MCE is  
162 ultimately a fairly imprecise metric, especially for the  $SSA_{405\text{nm}}$ .

163 However, we find a very strong relationship between the  $SSA_{405\text{nm}}$  and the total  $[OA]/[BC]$   
164 ratio (**Figure 1e**). This is consistent with the findings of Pokhrel et al. (2016), who observed  
165 something similar but over a smaller range of  $[OA]/[BC]$ . (Similarly strong relationships are  
166 observed for SSA values at 532 nm and 781 nm (**Figure S1**), or if the  $[NR-PM_{10}]/[BC]$  are used as  
167 OA averages 95% of the total NR- $PM_{10}$  mass.) Smaller  $[OA]/[BC]$  correspond to smaller  $SSA_{405\text{nm}}$   
168 values with a sigmoidal relationship observed. (Fit parameters for all fits shown are provided in  
169 **Table S1**.) There is similarly a very strong, sigmoidal relationship between the AAE and  
170  $MAC_{BC,405\text{nm}}$  and  $[OA]/[BC]$  (**Figure 1f,g**). The large increase in the  $MAC_{BC,405\text{nm}}$  indicates that  
171 BrC contributes substantially to the total absorption. The contributions of coating-induced  
172 enhancements and of BrC are discussed further in Sections 3.4.1 and 3.4.2. The larger range of  
173  $[OA]/[BC]$  and the greater number of individual burns considered here, compared to Pokhrel et al.  
174 (2016), allows for determination of more robust fits. Pokhrel et al. (2017) found that the absorption  
175 enhancement at 405 nm, determined from thermodenuder measurements, increased with  
176  $[OA]/[BC]$  up to  $[OA]/[BC] \sim 33$  (the largest value reported), consistent with our findings.

177 These observations demonstrate that the optical properties of the primary particles depend on the  
178 relative amount of OA versus BC. This is as expected because OA is generally more scattering,



179 compared to BC, and light absorbing OA (aka BrC) typically exhibits a much stronger wavelength  
180 dependence than BC. Based on these relationships, we divide the individual burns into different  
181 classes (**Table 1**). We have chosen to classify particles based on the observed SSA<sub>405nm</sub> values;  
182 use of [OA]/[BC] for classification yields largely similar results, given the strong relationship  
183 between the two. The dividing lines between classes are selected to yield six classes that span the  
184 entire range of SSA<sub>405nm</sub> values, from 0.23 (Class 1) to 0.97 (Class 6), with approximately equal  
185 numbers of individual burns in each class (ca. 8-10). Partitioning the observations into different  
186 particle classes facilitates interpretation of the photochemical evolution of the particles, to be  
187 discussed in future work. In addition, we find that use of the Class average properties versus MCE  
188 generally provides more representative fits to the observations (visually apparent in **Figure 1**, and  
189 supported by the reduced  $\chi^2$  for the fits).

### 190 **3.2 OA composition and volatility**

191 Variability in the bulk composition of the OA is characterized by the O:C and H:C atomic  
192 ratios and the fractional abundance ( $f_x$ ) of two marker ions,  $m/z = 44$  and  $m/z = 60$ . The  $f_{44}$  is  
193 complementary to O:C and larger values generally indicate a greater degree of oxygenation and  
194 the presence of carboxylic acids. The  $f_{60}$  is often taken as a marker ion for biomass burning, in  
195 particular a signature of levoglucosan and similar molecules (Schneider et al., 2006;Alfarra et al.,  
196 2007). The high resolution ion  $C_2H_4O_2^+$  contributes to and exhibits similar behavior as  $f_{60}$ ; the  
197 slope for  $f_{C_2H_4O_2^+}$  against  $f_{60}$  is 0.98. While it is known that properties such as  $f_{60}$  vary in different  
198 biomass burning samples (Schneider et al., 2006) or between near-source intercepts of different  
199 ambient plumes (Garofalo et al., 2019), the specific dependence on burn conditions or overall  
200 particle composition (e.g. [OA]/[BC]) has not been systematically explored to our knowledge.

201 The average  $f_{60} = 0.022 \pm 0.01$  ( $1\sigma$ ). The  $f_{60}$  values vary non-monotonically with [OA]/[BC],  
202 exhibiting a slight increase from Class 1 to Class 3 and then a decrease from Class 4 to Class 6  
203 (Figure 2a). This indicates that, while  $f_{60}$  is overall a useful marker ion for biomass burning, it  
204 cannot be used to distinguish between different burn conditions. The  $f_{44}$  generally decreases with  
205 [OA]/[BC] (Figure 2b;  $r^2 = 0.33$ .) However, the average  $f_{44}$  values for particle Classes 2-5 differ  
206 negligibly, suggesting that  $f_{44}$  might be useful in discriminating between extreme cases (e.g. Class  
207 1 versus Class 6), but that it is of limited general use in distinguishing between burn conditions  
208 and fuel types. The O:C atomic ratio (average =  $0.37 \pm 0.09$ ) exhibits similar behavior—expected



209 as  $f_{44}$  is generally related to O:C (Aiken et al., 2008)—with a general decrease as  $[OA]/[BC]$   
210 increases, although a comparably weaker correlation (Figure 2c;  $r^2 = 0.17$ ). The H:C (average =  
211  $1.76 \pm 0.05$ ) exhibits a weak, positive correlation with  $[OA]/[BC]$ , although the variability is slight  
212 (Figure 2d;  $r^2 = 0.27$ ).

213 The mass fraction of the OA that is composed of nitrated organics ( $f_{ON-OA} = [ON]/[OA]$ ) was  
214 determined using the HR-ToF-AMS measurements and the method of Kiendler-Scharr et al.  
215 (2016) (see the Supplemental Material for further details). The terminology nitrated organics (ON)  
216 includes contributions from both nitro and nitrate functional groups. The fraction of measured  
217 nitrate that was ON ( $f_{ON-N} = [ON]/([ON]+[NO_3^-])$ ) decreased with  $[OA]/[BC]$  and ranged from 0.91  
218 (Class 1) to 0.48 (Class 6) (**Figure S2a**). The Class-specific average  $f_{ON-OA}$  also decreased with  
219  $[OA]/[BC]$ , although by a much greater extent than the  $f_{ON-N}$ , ranging from 6.0% (Class 1) to 0.27%  
220 (Class 6) and (**Figure 2e**). There is a reasonably linear relationship between  $\log(f_{ON-OA})$  and  
221  $\log([OA]/[BC])$  ( $r^2 = 0.47$ ). This indicates that a larger proportion of ON species and  
222 functionalities are produced when particles are, on average, more BC-rich. This does not reflect  
223 differences in fuel nitrogen content as there is no relationship between fuel N and  $f_{ON-OA}$  (**Figure**  
224 **S2b**). Therefore, it seems that the relationship between  $f_{ON-OA}$  and  $[OA]/[BC]$  is related more so to  
225 the burn conditions than the fuel N content, although as with many other properties the relationship  
226 with  $[OA]/[BC]$  is clearer than with the MCE (**Figure S2c**).

227 The OA volatility is characterized as the ratio between the OA concentration after  
228 thermodenuding to that without thermodenuding (the mass fraction remaining,  $MFR_{OA}$ ). The  
229  $MFR_{OA}$  decreases as  $[OA]/[BC]$  increases (**Figure 2f**), indicating that the OA at lower  $[OA]/[BC]$   
230 is less volatile than the OA at higher values. This observation provides support for the proposal by  
231 Saleh et al. (2014) that less volatile, more absorbing species are preferentially formed under  
232 conditions where BC formation is favored, discussed further in Section 3.4.2. The relationship  
233 between  $MFR_{OA}$  and  $[OA]/[BC]$  is reasonably described by an exponential function.

### 234 3.3 BC Mixing State

235 As discussed above, the relative amounts of OA and BC vary greatly between fuel types and  
236 combustion conditions. However, the distribution of BC and OA between particles, and how this  
237 varies between very different burn conditions, has not been previously explored in detail to our



238 knowledge. The bulk average fraction of OA that is internally mixed with BC versus OA that is  
239 externally mixed from BC is determined using the HR-ToF-AMS and SP-AMS measurements.  
240 The HR-ToF-AMS quantifies OA independent of mixing state, whereas the SP-AMS (as operated  
241 here) quantifies only the OA that is internally mixed with BC. The fraction of OA that is internally  
242 mixed with BC ( $f_{OA,int}$ ) is:

$$243 \quad f_{OA,int} = \frac{[OA]_{SP-AMS}}{[OA]_{HR-ToF-AMS}} = \frac{[OA]_{int}}{[OA]_{tot}} \quad (5)$$

244 where the subscript *int* indicates the OA that is internally mixed with BC and the subscript *tot*  
245 indicates the total OA. The  $f_{OA,int}$  should range from 0 to 1. Related, the SP-AMS quantified the  
246 ratio between the OA that is internally mixed with BC and the BC concentration, referred to here  
247 as  $[OA]_{int}/[BC]$ . We find that  $f_{OA,int}$  decreases substantially as  $[OA]/[BC]$  increases, ranging from  
248  $f_{OA,int} = 0.4$  for Class 1 (low SSA) particles to  $f_{OA,int} = 0.01$  for Class 6 (high SSA) particles (**Figure**  
249 **3a**). The data are well-fit by a sigmoidal function. However, the amount of OA coating BC ( $R_{OA-BC}$   
250  $= [OA]_{int}/[BC]$ ) increases with the total  $[OA]/[BC]$ , also with a sigmoidal relationship (**Figure 3b**).  
251 Thus, while a smaller fraction of the total OA is internally mixed with BC for larger total  
252  $[OA]/[BC]$  the amount of OA that coats BC increases. Most likely this behavior reflects that BC  
253 and OA are generated with different efficiencies in different parts of the combusting biomass. BC  
254 is more efficiently generated from flaming combustion while OA is more efficiently generated  
255 from smoldering combustion. These observations demonstrate that the extent to which  
256 atmospheric models can assume that all OA is internally mixed with or externally mixed from BC  
257 at the point of emission will depend on the combustion conditions.

## 258 **3.4 Absorption enhancement and brown carbon**

### 259 **3.4.1 Coating-induced absorption enhancement**

260 Non- or weakly-absorbing coatings on black carbon particles can theoretically increase the  
261 absorption by BC (Fuller et al., 1999; Bond et al., 2006), an effect which has been confirmed by  
262 laboratory experiments (Lack et al., 2009; Shiraiwa et al., 2010; Cappa et al., 2012). The extent to  
263 which coatings on BC actually enhance absorption by BC in the atmosphere remains unclear. Some  
264 studies indicate minor coating-induced enhancements while others indicate substantial  
265 enhancements (Cappa et al., 2012; Healy et al., 2015; Liu et al., 2015; Peng et al., 2016; Zhang et al.,



266 2016;Liu et al., 2017;Cappa et al., 2019b). Understanding the nature of the coating-induced  
267 enhancement is important for quantifying the radiative impacts of BC (Jacobson, 2001;Bond et al.,  
268 2013). Further, these coating-induced absorption enhancements ( $E_{\text{abs,coat}}$ ) complicate the  
269 determination of brown carbon (BrC) absorption and the two must be separated. Here, we examine  
270 the extent to which coatings on BC for primary biomass burning particles enhance the BC  
271 absorption. Theoretically, the magnitude of  $E_{\text{abs,coat}}$  for an individual particle depends primarily on  
272 the coating thickness and secondarily on the size of the BC core (Bond et al., 2006; Fuller et al.,  
273 1999). Thus, the extent to which coatings enhance BC absorption for a given situation can be  
274 assessed through the relationship between the observed  $MAC_{\text{BC}}$  and the coating-to-core mass ratio  
275 ( $R_{\text{coat-rBC}} = [\text{NR-PM}]_{\text{int}}/[\text{BC}]$ , where *int* indicates that the coating material is internally mixed with  
276 BC). The expectation is that the  $MAC_{\text{BC}}$  increases with  $R_{\text{coat-BC}}$ .

277 However, absorption by BrC can also lead to an apparent increase in the normalized absorption  
278 with  $R_{\text{BC}}$  if the BrC abundance correlates with the total coating amount. Because BrC absorbs more  
279 strongly at shorter wavelengths, the wavelength-dependence of the  $MAC_{\text{BC}}$  to  $R_{\text{BC}}$  relationship can  
280 be used to further separate the influence of coating versus BrC absorption. The  $MAC_{\text{BC}}$  exhibits a  
281 wavelength-dependent relationship with  $R_{\text{coat-rBC}}$  for fresh biomass particles (405 nm, 532 nm and  
282 781 nm) (**Figure 4a-c**). The  $MAC_{\text{BC}}$  increases notably with  $R_{\text{coat-rBC}}$  at 405 nm and to a lesser extent  
283 at 532 nm. At 781 nm the  $MAC_{\text{BC}}$  is essentially independent of  $R_{\text{coat-rBC}}$  up to  $R_{\text{coat-rBC}}$  values as  
284 large as 10, but does exhibit some increase at  $R_{\text{coat-rBC}} > 10$ . However, this is most likely a result  
285 of absorption by OA at 781 nm and not indicative of an increase in the coating-induced  
286 enhancement, discussed further below. The wavelength dependence provides clear evidence of  
287 BrC absorption at shorter wavelengths.

288 That the  $MAC_{\text{BC}}$  at 781 nm is nearly independent of  $R_{\text{coat-rBC}}$  up to such large  $R_{\text{coat-rBC}}$  values  
289 indicates that there is a negligible coating-induced enhancement for the primary biomass particles.  
290 Our observations are consistent with McMeeking et al. (2014), who also investigated the  
291 relationship between the  $MAC_{\text{BC}}$  and  $R_{\text{coat-rBC}}$  for a primary biomass particles from multiple fuel  
292 types. Most likely, this lack of a substantial coating-induced enhancement results from a non-even  
293 distribution of non-BC mass across the population of BC particles (Fierce et al., 2016;Liu et al.,  
294 2017) and from the morphology of BC-containing particles not conforming to an idealized core-  
295 shell structure (Adachi et al., 2010). The influence of photochemical aging on the coating-induced  
296 enhancement will be examined in future work.



297 The relationship between  $MAC_{BC}$  and the coating amount ( $R_{coat-rBC}$ ) can be contrasted with the  
298 relationship between  $MAC_{BC}$  and the total  $[OA]/[BC]$ . At all three wavelengths the  $MAC_{BC}$  exhibit  
299 strong, sigmoidal relationships with  $[OA]/[BC]$  (**Figure 4d-f**). That  $MAC_{BC,781nm}$  exhibits such a  
300 clear relationship with  $[OA]/[BC]$  suggests that even the small apparent coating-induced  
301 enhancement, implied above from the very weak with  $R_{coat-rBC}$ , is largely driven by absorption by  
302 BrC rather than from the impact of coating on BC. Pokhrel et al. (2017) found that the absorption  
303 enhancement, determined from thermodenuder measurements, increased notably with  $[OA]/[BC]$   
304 up to  $[OA]/[BC] \sim 33$  at 405 nm (the largest value reported by them), but by much less at 660 nm,  
305 consistent with our findings.

306 The observations allow for determination of wavelength-dependent  $MAC_{BC}$  values for pure BC  
307 ( $MAC_{BC,pure}$ ) for each wavelength by extrapolation of the  $MAC_{BC}$  versus  $[OA]/[rBC]$  ratio to zero  
308 using sigmoid fits. Since the  $R_{coat-rBC}$  correlates reasonably with  $[OA]/[BC]$  (**Figure 3b**),  
309 extrapolation against  $[OA]/[BC]$  to zero effectively removes both contributions from BrC and any  
310 coating-induced enhancement. The derived  $MAC_{BC,pure}$  values are  $11.8 \text{ m}^2 \text{ g}^{-1}$  at 405 nm,  $8.8 \text{ m}^2$   
311  $\text{g}^{-1}$  at 532 nm and  $5.5 \text{ m}^2 \text{ g}^{-1}$  at 781 nm, with estimated fit-based uncertainties of  $\sim 10\%$ . The  
312 absolute uncertainties on the  $MAC_{BC,pure}$  are primarily dependent on the uncertainty in the  $b_{abs}$  and  
313  $[rBC]$  measurements, and are  $\sim 35\%$ . The derived  $MAC_{BC}$  values are very similar to those recently  
314 reported by Forestieri et al. (2018) for fresh BC particles:  $MAC_{BC,pure} = 11.9 \text{ m}^2 \text{ g}^{-1}$  at 405 nm and  
315  $8.8 \text{ m}^2 \text{ g}^{-1}$  at 532 nm, with an extrapolated value at 781 nm of  $5.7 \text{ m}^2 \text{ g}^{-1}$ . The value at 532 nm is  
316 somewhat higher than that suggested by Bond and Bergstrom (2006) ( $7.75 \text{ m}^2 \text{ g}^{-1}$  at 532 nm). Our  
317 derived  $MAC_{BC,pure}$  values yield an  $AAE = 1.17$ , determined from a fit to the three wavelengths. An  
318  $AAE$  close to unity indicates absorption is dominated by BC, as expected.

### 319 3.4.2 Primary brown carbon absorption

320 The absorption due to brown carbon is determined by difference as:

$$321 \quad b_{abs,BrC} = b_{abs,obs} - MAC_{BC,pure} \cdot [BC] \cdot E_{abs,coat} \quad (6)$$

322 where  $b_{abs,BrC}$  is the absorption due to BrC specifically. Importantly, the use of study-specific  
323  $MAC_{BC,pure}$  values serves to reduce systematic biases in the  $b_{abs,BrC}$ , compared to direct use of  
324 literature  $MAC_{BC,pure}$  values. Assuming  $E_{abs,coat} = 1$  provides an upper limit on the BrC absorption,  
325 which we note is likely most appropriate for the particles sampled here, as discussed in the previous



326 section. Therefore, we use the upper-limit values throughout the analysis that follows, unless  
327 otherwise stated. However, a lower limit for BrC absorption can be determined at 405 nm and 532  
328 nm assuming that all of the enhancement at 781 nm results from coatings and not from BrC. The  
329 resulting  $E_{\text{abs,obs}}$  ( $= MAC_{\text{BC,obs}}/MAC_{\text{BC,pure}}$ ) at 781 nm averages 1.19 for  $R_{\text{BC-coat}} < 10$ . Using  $E_{\text{abs,coat}}$   
330  $= 1.19$  in Eqn. 7 yields a lower limit for the BrC absorption at the two shorter wavelengths,  
331 appropriate since  $E_{\text{abs,coat}}$  generally has only a small wavelength dependence. A fit to the coating-  
332 corrected (lower-limit) versus upper-limit  $b_{\text{abs,BrC}}$  yields a slope of 0.97 at 405 nm and 0.88 at 532  
333 nm (**Figure S3**). The smaller difference at 405 nm results from the fractional contribution of BrC  
334 to the total absorption being larger at this wavelength.

335 Brown carbon-specific mass absorption coefficients ( $MAC_{\text{BrC}}$ ) are determined as the ratio  
336 between  $b_{\text{abs,BrC}}$  and the total OA concentration:

$$337 \quad MAC_{\text{BrC}} = \frac{b_{\text{abs,BrC}}}{[\text{OA}]} \quad (7)$$

338 The  $MAC_{\text{BrC}}$  values from Eqn. 7 are bulk-average values, and do not account for different  
339 molecules and classes of molecules likely having different absorptivities. Uncertainties in the  
340  $MAC_{\text{BrC}}$  values are determined by error propagation. Similarly, an AAE value for just the brown  
341 carbon ( $AAE_{\text{BrC}}$ ) can be calculated using wavelength pairs as:

$$342 \quad AAE_{\text{BrC}} = -\log\left(\frac{b_{\text{abs,BrC},\lambda_1}}{b_{\text{abs,BrC},\lambda_2}}\right) / \log\left(\frac{\lambda_1}{\lambda_2}\right); \quad (8)$$

343 The geometric averages of the  $MAC_{\text{BrC}}$  values are  $0.76_{-0.35}^{+0.65} \text{ m}^2 \text{ g}^{-1}$ ,  $0.21_{-0.13}^{+0.36} \text{ m}^2 \text{ g}^{-1}$ ,  $0.056_{-0.04}^{+0.15}$   
344  $\text{m}^2 \text{ g}^{-1}$  at 405 nm, 532 nm and 781 nm, with uncertainties the  $1\sigma$  burn-to-burn variability. The  
345  $MAC_{\text{BrC}}$  values vary between classes, generally increasing as the  $[\text{OA}]/[\text{BC}]$  ratio decreases at all  
346 wavelengths (shown for 405 nm in **Figure 5a**). For example, the average  $MAC_{405\text{nm}} = 2.3 \pm 1 \text{ m}^2$   
347  $\text{g}^{-1}$  for Class 1 and  $0.35 \pm 0.09 \text{ m}^2 \text{ g}^{-1}$  for Class 6. Although the uncertainties on the derived  $MAC_{\text{BrC}}$   
348 increase substantially as  $[\text{OA}]/[\text{BC}]$  decreases—because BrC absorption contributes to a smaller  
349 extent at longer wavelengths—the observations nonetheless indicate that the BrC absorptivity  
350 depends on the combustion conditions. The relationship at 405 nm is well-described by a sigmoidal  
351 function in log-log space, with limiting values of  $0.35 \text{ m}^2 \text{ g}^{-1}$  at large  $[\text{OA}]/[\text{BC}]$  and  $11.2 \text{ m}^2 \text{ g}^{-1}$   
352 at small  $[\text{OA}]/[\text{BC}]$ . That the extrapolated zero  $[\text{OA}]/[\text{BC}]$  limit for  $MAC_{\text{BrC}}$  is similar to pure BC  
353 suggests an evolution of BrC towards having properties similar to BC when the overall  $[\text{OA}]$



354 content is small. Such behavior is consistent with Saleh et al. (2018), who argue that there is a  
355 continuum of BrC properties that depends on the combustion conditions, as demonstrated in that  
356 study for low-temperature benzene and toluene combustion. The range of the observed  $MAC_{BrC}$   
357 values here encompass many previous measurements, summarized in **Table S3**. This likely reflects  
358 the wide diversity of fuel types and burn conditions considered here, as exemplified by the very  
359 large range of  $[OA]/[BC]$ .

360 Estimated values of the imaginary component of the refractive index for BrC ( $k_{BrC}$ ) are determined  
361 from Mie theory via optical closure (Zhang et al., 2016), assuming a real part of the refractive  
362 index of 1.5 and a particle diameter of 150 nm, a typical value for these experiments. Imaginary  
363 RI values are of use in atmospheric models for calculation of BrC absorption. There is a linear  
364 relationship between  $MAC_{BrC}$  and  $k_{BrC}$  (**Figure S4a**). Thus, the  $k_{BrC}$  exhibits a similar correlation  
365 with  $[OA]/[BC]$  as does the  $MAC_{BrC}$  (**Figure 5a**).

366 The wavelength-dependence of absorption, i.e. the  $AAE_{405-532}$ , also varies with  $[OA]/[BC]$ , in this  
367 case with a positive relationship between the two (**Figure 5b**). The relationship is reasonably  
368 described by a sigmoidal function. This implies that, while the  $MAC_{BrC}$  varies inversely with  
369  $[OA]/[BC]$  at all wavelengths, the exact variation is wavelength dependent. The  $AAE_{405-532}$   
370 relationship with  $[OA]/[BC]$  is well-described by a sigmoidal function (versus  $\log([OA]/[BC])$ ),  
371 with limiting values of 10.4 at large  $[OA]/[BC]$  and 1.3 at small  $[OA]/[BC]$ . The wavelength-  
372 dependence of the  $k_{BrC}$  ( $w_{BrC}$ ) are also calculated, to facilitate comparison with the literature, as:

$$373 \quad w_{BrC} = -\log\left(\frac{k_{BrC,\lambda 1}}{k_{BrC,\lambda 2}}\right) / \log\left(\frac{\lambda 1}{\lambda 2}\right) \quad (9)$$

374 The  $w_{BrC}$  exhibit a similar dependence on  $[OA]/[BC]$  as the  $AAE_{BrC}$ , as the  $w_{BrC}$  and  $AAE_{BrC}$  are  
375 linearly related, albeit with some scatter (**Figure S4b**;  $r^2 = 0.97$ ).

376 Our observations support the results of Saleh et al. (2014), who also found a relationship between  
377 the  $k_{BrC,405nm}$  and  $[OA]/[BC]$ . However, our analysis substantially extends the range of  $[OA]/[BC]$   
378 values investigated in that work (they considered  $[OA]/[BC]$  from only ca. 2 to 170). In the overlap  
379 region between our two studies the  $k_{BrC,405nm}$  agree reasonably well over the range  $2 < [OA]/[BC]$   
380  $< 50$ , but the  $k_{BrC,405nm}$  from Saleh et al. (2014) are smaller than observed here above  $[OA]/[BC] =$   
381 50. Importantly, our results demonstrate that the linear fit suggested by Saleh et al. (2014) for  
382  $MAC_{BrC}$  is only appropriate over the range of values they considered and that a sigmoidal provides



383 for a more robust relationship over a wider range of  $[OA]/[BC]$ . Related, the wider range of  
384  $[OA]/[BC]$  enables more robust determination of the functional dependence of the wavelength-  
385 dependence of absorption ( $w_{BrC}$ ), with overall larger  $w_{BrC}$  values and a larger plateau at high  
386  $[OA]/[BC]$  compared to the fit by Saleh et al. (2014).

387 The  $MAC_{BrC}$  values also correlate with the nitrated organic fraction of OA, the latter of which, as  
388 noted above, also correlates with the  $[OA]/[BC]$  (**Figure 6a**). This observation suggests that  
389 organic nitrate and nitro functionalities may be at least somewhat responsible for the increase in  
390 absorption. Laskin et al. (2018) performed offline molecular level analyses of primary OA  
391 collected during FIREX. They found that nitroaromatics and N-containing polycyclic aromatic  
392 hydrocarbons (PAHs) contribute notably to the total light absorption by BrC, although there are  
393 many non-N-containing species that also contribute to BrC absorption. The variability between  
394 particle Classes is consistent with the results of Lin et al. (2016), which show that the abundance  
395 of N-containing chromophores varies between particles produced from different biomass fuels.  
396 Additionally Mohr et al. (2013) observed a relationship between the concentration of nitrated  
397 phenols and short-wavelength absorption by BrC, although it is possible that for their  
398 measurements these species were produced from chemical processing, as opposed to being directly  
399 emitted. Altogether, our results provide support for the idea that nitrated organic functionalities  
400 are an important contributor to BrC absorption. However, it is very likely that other functional  
401 groups also contribute to the total absorption.

402 The  $MAC_{BrC,405nm}$  exhibits an inverse correlation with the  $f_{60}/f_{44}$  ratio of the OA, although there is  
403 substantial scatter in the  $f_{60}/f_{44}$  ratio for a given particle class (**Figure 6b**). (The  $f_{44}$  and  $f_{60}$  have no  
404 discernable relationship.) The observed  $MAC_{BrC,405nm}$  relationship with  $f_{60}/f_{44}$  is opposite that  
405 reported by Lack et al. (2013) for ambient measurements of particles a biomass burning plume,  
406 who find a reasonable positive correlation. This difference in behavior results from our sampling  
407 primary particles directly—thereby focusing on the inherent variability in the properties of the  
408 emitted particles—while Lack et al. (2013) sampled ambient particles. For ambient sampling, the  
409 observed relationship will be sensitive to mixing of biomass burning particles with background or  
410 aged biomass particles, which are known to have a smaller  $f_{60}$  (Cubison et al., 2011). Thus, the  
411 relationship observed by Lack et al. (2013) can best be viewed as a mixing line between the fresh  
412 primary particles (having large  $MAC_{BrC,405nm}$  and large  $f_{60}/f_{44}$ ) and background or aged biomass



413 particles (having small  $MAC_{BrC,405nm}$  and small  $f_{60/f44}$ ), rather than providing information on the  
414 inherent variability in the absorptivity of the fresh particles.

### 415 3.5 Size distributions

416 Total particle mobility size distributions and BC-only size distributions were measured (**Figure**  
417 **7**). Primary particle size distributions are important parameters specified in regional and global  
418 models. The number-weighted and volume-weighted size distribution are generally described by  
419 either one or two log-normal modes for individual burns; a two-mode fit provides a more robust  
420 solution across all modes. The mass-weighted BC size distributions are similarly described by one  
421 or two log-normal modes. A fit to the average number-weighted distribution across all particle  
422 classes yields geometric median diameters ( $d_{p,N}$ ) and widths ( $\sigma_g$ ) of 60.3 nm and 1.76, respectively,  
423 for the smaller mode and 153 nm and 1.64 for the larger mode (**Figure 8**). The amplitude of the  
424 smaller mode is 4.6 times the larger mode. A single mode fit yields  $d_{p,N} = 68$  nm and  $\chi_g = 1.93$ ,  
425 although the fit is poorer. Mann et al. (2014) report  $d_{p,N}$  values used by a variety of global models  
426 for biofuels. The models tend to use either 80 nm or 150 nm, although a few use other values (30  
427 nm, 60 nm, 100 nm). Those using 80 nm typically use  $\sigma_g = 1.80$  while those using 150 nm typically  
428 use  $\sigma_g = 1.59$ , although there are exceptions. Our observations indicate that use of a bimodal  
429 distribution within models would be more representative, but that a single mode can do acceptably.  
430 We find that the volume-weighted distribution calculated from a single-mode fit to the number-  
431 weighted distribution is similar to the observed volume-weighted distribution (**Figure 8**). Thus,  
432 the use of a single-mode to represent biomass burning size distributions thus appears acceptable,  
433 so long as the appropriate parameters are used. In this context, the widths of the distribution used  
434 by the various global models appear somewhat too small. However, we note that the microphysics  
435 occurring in the fresh smoke sampled here, which will govern the size distributions, may differ  
436 from that in atmospheric plumes.

437 The average BC-specific mass-weighted size distribution mode is at 148 nm (**Figure 8**). A  
438 bimodal fit yields values for the mass median diameter ( $d_{p,M}$ ) and  $\sigma_g$  of 137.2 nm and 1.62,  
439 respectively, for the smaller mode and 197.1 nm and 1.24 for the larger mode, with most of the  
440 mass contained in the smaller mode. May et al. (2014) report  $d_{p,M}$  from laboratory biomass  
441 combustion ranging from 140-190 nm, averaging 170 nm. Their average is somewhat larger than



442 ours, likely reflecting differences in the exact fuels sampled. The mode diameter for the BC-  
443 specific distribution is especially smaller than observed for biomass burning particles from some  
444 ambient observations, which tend to give values closer to 200 nm (Schwarz et al., 2008;Kondo et  
445 al., 2011;Sahu et al., 2012;May et al., 2014;Cappa et al., 2019b). This difference between lab and  
446 field observations was also noted by May et al. (2014). We speculate that the influence of  
447 coagulation may be suppressed in our experiments relative to what occurs in the atmosphere due  
448 to slower overall dilution, leading to smaller BC size distributions. To the extent this is the reason  
449 for the difference, the total particle distributions would also be biased towards too small particles,  
450 compared to the atmosphere. However, there is no relationship between  $d_{p,N}$  and the total particle  
451 number concentration for our experiments. Formation of secondary aerosol in the near-field of a  
452 sampled ambient plume could also contribute to this difference.

453 There is substantial variability between individual burns within a given particle Class in terms  
454 of the shape of the size distributions (**Figure 7**). This variability is most evident for Class 1, 2 and  
455 5, but present for all Classes. Nonetheless, the number-weighted mean diameter ( $d_{p,N,\text{mean}}$ ) appears  
456 to decrease somewhat with MCE (**Figure 9**;  $r^2 = 0.38$ ). However, the relationship is largely driven  
457 by the Class 6 particles, which generally have lower MCE values, having larger  $d_{p,N,\text{mean}}$  values. A  
458 lack of any particularly clear relationship is consistent with Hosseini et al. (2010), who observed  
459 the  $d_{p,N,\text{mean}}$  to exhibit a complex relationship with combustion conditions. The  $d_{p,N,\text{mean}}$  varies non-  
460 monotonically with [OA]/[BC], with particle size first decreasing slightly as [OA]/[BC] increases  
461 (from Class 1 to Class 3) and then increasing with further increases in [OA]/[BC] (from Class 4 to  
462 Class 6) (**Figure 9**). This is despite the notable burn-to-burn variability. It is important to note that  
463 the mobility-based size is particle shape-dependent; very BC-rich particles are more likely to have  
464 non-spherical shapes and thus have larger mobility diameters. This could explain the minimum in  
465  $d_{p,N}$  around Class 3 particles, for which [OA]/[BC] = 10.

466 Some of the variability within a class appears related to the presence of different fuel types  
467 within a class. Number-weighted and BC-specific mass-weighted size distributions by fuel type  
468 are shown in **Figure 10**. For the number-weighted distributions, leaf litter and rotten logs exhibit  
469 the greatest variability between different burns, although we note that multiple burns were not  
470 performed for all fuels. The shapes of the leaf litter, peat and “other” fuel types differ most notably  
471 from the other fuel types, with the presence of more than one mode more apparent. (The “other”  
472 category here includes non-traditional biofuels, specifically building materials and excelsior.) For



473 the BC-specific size distributions, the litter, canopy, and duff exhibited the greatest intra-fuel  
474 variability. For most fuels, the BC-specific distribution peaks around 150 nm, as noted above.  
475 However, for a subset of burns (eight of them) the BC-specific distribution peaks around 100 nm  
476 (**Figure 10**). These small BC-mode distributions occur for the OA-rich particle classes 4, 5 and 6  
477 (**Figure 7**), although there is no clear pattern to their occurrence.

#### 478 **4 Conclusions and Implications**

479 Measurements of primary particles produced from combustion of a variety of biomass fuel  
480 types indicate the optical, physical, and chemical properties of the emitted particles exhibit wide  
481 variability. We show that variability in many optical properties (e.g. single scatter albedo,  
482 wavelength dependence of absorption, mass absorptivity of black and brown carbon) is directly  
483 linked to the [OA]/[BC] ratio of the emitted particles; the relationships with [OA]/[BC] are much  
484 stronger than with the commonly used modified combustion efficiency, and mathematical  
485 relationships between the various properties are determined. However, the absorption  
486 enhancement due to coating of BC (the so-called “lensing” effect) is shown to be negligible and  
487 essentially independent of the amount of coating up to large coating-to-BC mass ratios. The brown  
488 carbon mass absorptivity correlates with the nitrated organic fraction of OA, suggesting that  
489 nitrated organic species contribute to BrC absorption. Many bulk chemical properties (i.e. O:C,  
490 H:C, and the relative concentrations of key marker ions such as  $f_{60}$ ) exhibit limited dependence on  
491 the burn conditions and the [OA]/[BC] ratio. However, both the OA volatility and nitrated organic  
492 fraction of OA decrease with [OA]/[BC]. The fraction of OA that is internally mixed with BC was  
493 shown to decrease strongly with the [OA]/[BC] ratio, from nearly all OA being internally mixed  
494 with BC when the particles are overall BC-rich to only a few percent of OA being mixed with BC  
495 when OA dominates. Yet, the relative amount of OA coating the BC increases with [OA]/[BC];  
496 that is, when more of the OA is externally mixed from BC those particles that do contain BC  
497 nonetheless have thicker OA coatings. The observed total particle size distributions are reasonably  
498 well described by a single log-normal mode, but are better fit using a bimodal distribution. The  
499 BC-specific size distributions are similarly best fit using a bimodal distribution, although a single  
500 mode provides a reasonable representation. The dependence of the geometric median mobility  
501 diameter on the burn conditions or particle state (i.e. the [OA]/[BC]) is complicated by the mobility  
502 diameter being sensitive to variations in particle shape, which depend on the [OA]/[BC] ratio.  
503 Overall, these results expand on previous observations of primary biomass burning particle



504 properties, considering a wider range of [OA]/[BC] and associated properties. Further, they  
505 provide a foundation for understanding the post-emission evolution of biomass burning smoke due  
506 to photochemical oxidation as discussed in Lim et al. (2019).

## 507 **5 Data Availability**

508 All data are available from the NOAA FIREX-AQ data repository  
509 (<https://esrl.noaa.gov/csd/projects/firex/firelab/>). This includes a summary of the fuel types used  
510 for each burn and the measurement time-series for each burn. The primary particle averages used  
511 in this work are additionally collected in the UC DASH data repository (Cappa et al., 2019a).

## 512 **6 Author Contributions**

513 CDC and JHK designed the experiments. CDC, CYL, and DHH carried out the measurements  
514 and data processing. CDC, CDM, and CYL analyzed data. CDC and CDM wrote the manuscript,  
515 with contributions from all co-authors.

## 516 **7 Acknowledgements**

517 This work was supported by the National Oceanic and Atmospheric Administration  
518 Atmospheric Chemistry, Carbon Cycle & Climate Program, awards NA16OAR4310111 and  
519 NA16OAR4310112. CYL was additionally supported by the National Science Foundation  
520 Graduate Research Fellowship Program. The entire FIREX team, especially Bob Yokelson and  
521 Jim Roberts and the staff of the Missoula Fire Sciences Laboratory, are acknowledged for their  
522 assistance. Putting together the community inlet was a community effort—thank you to all who  
523 contributed. Shuka Schwarz and Gavin McMeeking are also thanked for their assistance with the  
524 SP2.



## 525 8 References

- 526 Adachi, K., Chung, S. H., and Buseck, P. R.: Shapes of soot aerosol particles and implications for  
527 their effects on climate, *J. Geophys. Res.*, 115, D15206, <https://doi.org/10.1029/2009jd012868>,  
528 2010.
- 529 Adler, G., Flores, J. M., Abo Riziq, A., Borrmann, S., and Rudich, Y.: Chemical, physical, and  
530 optical evolution of biomass burning aerosols: a case study, *Atmos. Chem. Phys.*, 11, 1491-1503,  
531 <https://doi.org/10.5194/acp-11-1491-2011>, 2011.
- 532 Aiken, A. C., Decarlo, P. F., Kroll, J. H., Worsnop, D. R., Huffman, J. A., Docherty, K. S., Ulbrich,  
533 I. M., Mohr, C., Kimmel, J. R., Sueper, D., Sun, Y., Zhang, Q., Trimborn, A., Northway, M.,  
534 Ziemann, P. J., Canagaratna, M. R., Onasch, T. B., Alfarra, M. R., Prevot, A. S. H., Dommen, J.,  
535 Duplissy, J., Metzger, A., Baltensperger, U., and Jimenez, J. L.: O/C and OM/OC ratios of primary,  
536 secondary, and ambient organic aerosols with high-resolution time-of-flight aerosol mass  
537 spectrometry, *Environ. Sci. Technol.*, 42, 4478-4485, <https://doi.org/10.1021/es703009q>, 2008.
- 538 Alfarra, M. R., Prevot, A. S. H., Szidat, S., Sandradewi, J., Weimer, S., Lanz, V. A., Schreiber, D.,  
539 Mohr, M., and Baltensperger, U.: Identification of the Mass Spectral Signature of Organic  
540 Aerosols from Wood Burning Emissions, *Environmental Science & Technology*, 41, 5770-5777,  
541 <https://doi.org/10.1021/es062289b>, 2007.
- 542 Andreae, M. O., and Merlet, P.: Emission of trace gases and aerosols from biomass burning, *Global*  
543 *Biogeochemical Cycles*, 15, 955-966, <https://doi.org/doi:10.1029/2000GB001382>, 2001.
- 544 Bluvshstein, N., Lin, P., Flores, J. M., Segev, L., Mazar, Y., Tas, E., Snider, G., Weagle, C., Brown,  
545 S. S., Laskin, A., and Rudich, Y.: Broadband optical properties of biomass-burning aerosol and  
546 identification of brown carbon chromophores, *Journal of Geophysical Research: Atmospheres*,  
547 122, 5441-5456, <https://doi.org/doi:10.1002/2016JD026230>, 2017.
- 548 Bond, T. C., and Bergstrom, R. W.: Light absorption by carbonaceous particles: An investigative  
549 review, *Aerosol Science and Technology*, 40, 27-67,  
550 <https://doi.org/10.1080/02786820500421521>, 2006.
- 551 Bond, T. C., Habib, G., and Bergstrom, R. W.: Limitations in the enhancement of visible light  
552 absorption due to mixing state, *J. Geophys. Res.-Atmos.*, 111,  
553 <https://doi.org/10.1029/2006JD007315>, 2006.
- 554 Bond, T. C., Doherty, S. J., Fahey, D. W., Forster, P. M., Berntsen, T., DeAngelo, B. J., Flanner,  
555 M. G., Ghan, S., Kärcher, B., Koch, D., Kinne, S., Kondo, Y., Quinn, P. K., Sarofim, M. C.,  
556 Schultz, M. G., Schulz, M., Venkataraman, C., Zhang, H., Zhang, S., Bellouin, N., Guttikunda, S.  
557 K., Hopke, P. K., Jacobson, M. Z., Kaiser, J. W., Klimont, Z., Lohmann, U., Schwarz, J. P.,  
558 Shindell, D., Storelvmo, T., Warren, S. G., and Zender, C. S.: Bounding the role of black carbon  
559 in the climate system: A scientific assessment, *Journal of Geophysical Research: Atmospheres*,  
560 118, 1-173, <https://doi.org/10.1002/jgrd.50171>, 2013.
- 561 Bruns, E. A., Perraud, V., Zelenyuk, A., Ezell, M. J., Johnson, S. N., Yu, Y., Imre, D., Finlayson-  
562 Pitts, B. J., and Alexander, M. L.: Comparison of FTIR and Particle Mass Spectrometry for the  
563 Measurement of Particulate Organic Nitrates, *Environmental Science & Technology*, 44, 1056-  
564 1061, <https://doi.org/10.1021/es9029864>, 2010.



- 565 Canagaratna, M. R., Jayne, J. T., Jimenez, J. L., Allan, J. D., Alfarra, M. R., Zhang, Q., Onasch,  
566 T. B., Drewnick, F., Coe, H., Middlebrook, A., Delia, A., Williams, L. R., Trimborn, A. M.,  
567 Northway, M. J., DeCarlo, P. F., Kolb, C. E., Davidovits, P., and Worsnop, D. R.: Chemical and  
568 microphysical characterization of ambient aerosols with the Aerodyne aerosol mass spectrometer,  
569 *Mass Spectrometry Reviews*, 26, 185-222, <https://doi.org/10.1002/mas.20115>, 2007.
- 570 Cappa, C. D., Onasch, T. B., Massoli, P., Worsnop, D., Bates, T. S., Cross, E., Davidovits, P.,  
571 Hakala, J., Hayden, K., Jobson, B. T., Kolesar, K. R., Lack, D. A., Lerner, B., Li, S. M., Mellon,  
572 D., Nuaanman, I., Olfert, J., Petaja, T., Quinn, P. K., Song, C., Subramanian, R., Williams, E. J.,  
573 and Zaveri, R. A.: Radiative absorption enhancements due to the mixing state of atmospheric black  
574 carbon, *Science*, 337, 1078-1081, <https://doi.org/10.1126/science.1223447>, 2012.
- 575 Cappa, C. D., Lim, C. Y., Hagan, D. H., and Kroll, J. H.: Measurements from the Fire Influence  
576 on Regional and Global Environments Experiment (FIREX) Fire Lab Mini Chamber Experiment,  
577 UC Davis DASH, Dataset, version 1, <https://doi.org/10.25338/B8CK5N>, 2019a.
- 578 Cappa, C. D., Zhang, X., Russell, L. M., Collier, S., Lee, A. K. Y., Chen, C.-L., Betha, R., Chen,  
579 S., Liu, J., Price, D. J., Sanchez, K. J., McMeeking, G., Williams, L. R., Onasch, T. B., Worsnop,  
580 D. R., Abbatt, J., and Zhang, Q.: Light absorption by ambient black and brown carbon and its  
581 dependence on black carbon coating state for two California, USA cities in winter and summer,  
582 *Journal of Geophysical Research-Atmospheres*, <https://doi.org/10.1029/2018JD029501>, 2019b.
- 583 Chakrabarty, R. K., Moosmüller, H., Chen, L. W. A., Lewis, K., Arnott, W. P., Mazzoleni, C.,  
584 Dubey, M. K., Wold, C. E., Hao, W. M., and Kreidenweis, S. M.: Brown carbon in tar balls from  
585 smoldering biomass combustion, *Atmospheric Chemistry and Physics*, 10, 6363-6370,  
586 <https://doi.org/10.5194/acp-10-6363-2010>, 2010.
- 587 Chen, Y., and Bond, T. C.: Light absorption by organic carbon from wood combustion, *Atmos.*  
588 *Chem. Phys.*, 10, 1773-1787, <https://doi.org/10.5194/acp-10-1773-2010>, 2010.
- 589 Coggon, M. M., Lim, C. Y., Koss, A. R., Sekimoto, K., Yuan, B., Cappa, C. D., Kroll, J. H.,  
590 Selimovic, V., Zarzana, K. J., Brown, S. S., Roberts, J. M., Müller, M., Yokelson, R. J., Wisthaler,  
591 A., Krechmer, J., Jimenez, J. L., De Gouw, J., and Warneke, C.: OH-chemistry of volatile organic  
592 compounds emitted from laboratory and ambient biomass burning smoke: Influence of furans and  
593 oxygenated aromatics on ozone and secondary VOC formation., *Atmos. Chem. Phys. Discuss.*,  
594 <https://doi.org/10.5194/acp-2019-516>, 2019.
- 595 Collier, S., Williams, L. R., Onasch, T. B., Cappa, C. D., Zhang, X., Russell, L. M., Chen, C.-L.,  
596 Sanchez, K. J., Worsnop, D. R., and Zhang, Q.: Influence of emissions and aqueous processing on  
597 particles containing black carbon in a polluted urban environment: Insights from a soot particle –  
598 aerosol mass spectrometer, *Journal of Geophysical Research-Atmospheres*, 123, 6648-6666,  
599 <https://doi.org/10.1002/2017JD027851>, 2018.
- 600 Cubison, M. J., Ortega, A. M., Hayes, P. L., Farmer, D. K., Day, D., Lechner, M. J., Brune, W. H.,  
601 Apel, E., Diskin, G. S., Fisher, J. A., Fuelberg, H. E., Hecobian, A., Knapp, D. J., Mikoviny, T.,  
602 Riemer, D., Sachse, G. W., Sessions, W., Weber, R. J., Weinheimer, A. J., Wisthaler, A., and  
603 Jimenez, J. L.: Effects of aging on organic aerosol from open biomass burning smoke in aircraft  
604 and laboratory studies, *Atmos. Chem. Phys.*, 11, 12049-12064, <https://doi.org/10.5194/acp-11-12049-2011>, 2011.



- 606 Fierce, L., Bond, T. C., Bauer, S. E., Mena, F., and Riemer, N.: Black carbon absorption at the  
607 global scale is affected by particle-scale diversity in composition, *Nat. Comm.*, 7,  
608 <https://doi.org/10.1038/ncomms12361>, 2016.
- 609 Forestieri, S. D., Helgestad, T. M., Lambe, A. T., Renbaum-Wolff, L. H., Lack, D. A., Massoli,  
610 P., Cross, E. S., Dubey, M. K., Mazzoleni, C., Olfert, J., Freedman, A., Davidovits, P., Onasch, T.  
611 B., and Cappa, C. D.: Measurement and modeling of the multi-wavelength optical properties of  
612 uncoated flame-generated soot, *Atmos. Chem. Phys.*, 18, 12141-12159,  
613 <https://doi.org/10.5194/acp-18-12141-2018>, 2018.
- 614 Forrister, H., Liu, J., Scheuer, E., Dibb, J., Ziemba, L., Thornhill, K. L., Anderson, B., Diskin, G.,  
615 Perring, A. E., Schwarz, J. P., Campuzano-Jost, P., Day, D. A., Palm, B. B., Jimenez, J. L., Nenes,  
616 A., and Weber, R. J.: Evolution of brown carbon in wildfire plumes, *Geophysical Research Letters*,  
617 42, 4623-4630, <https://doi.org/10.1002/2015GL063897>, 2015.
- 618 Fuller, K. A., Malm, W. C., and Kreidenweis, S. M.: Effects of mixing on extinction by  
619 carbonaceous particles, *J. Geophys. Res.-Atmos.*, 104, 15941-15954,  
620 <https://doi.org/10.1029/1998jd100069>, 1999.
- 621 Garofalo, L. A., Pothier, M. A., Levin, E. J. T., Campos, T., Kreidenweis, S. M., and Farmer, D.  
622 K.: Emission and Evolution of Submicron Organic Aerosol in Smoke from Wildfires in the  
623 Western United States, *ACS Earth and Space Chem.*, 3, 1237-1247,  
624 <https://doi.org/10.1021/acsearthspacechem.9b00125>, 2019.
- 625 Healy, R., Wang, J., Jeong, C. H., Lee, A., Willis, M., Jaroudi, E., Zimmerman, N., Hilker, N.,  
626 Murphy, M., and Eckhardt, S.: Light-absorbing properties of ambient black carbon and brown  
627 carbon from fossil fuel and biomass burning sources, *Journal of Geophysical Research:*  
628 *Atmospheres*, 120, 6619-6633, 2015.
- 629 Hoffer, A., Gelencser, A., Guyon, P., Kiss, G., Schmid, O., Frank, G. P., Artaxo, P., and Andreae,  
630 M. O.: Optical properties of humic-like substances (HULIS) in biomass-burning aerosols,  
631 *Atmospheric Chemistry and Physics*, 6, 3563-3570, 2006.
- 632 Hoffer, A., Tóth, A., Nyirő-Kósa, I., Pósfai, M., and Gelencsér, A.: Light absorption properties of  
633 laboratory-generated tar ball particles, *Atmos. Chem. Phys.*, 16, 239-246,  
634 <https://doi.org/10.5194/acp-16-239-2016>, 2016.
- 635 Hosseini, S., Li, Q., Cocker, D., Weise, D., Miller, A., Shrivastava, M., Miller, J. W., Mahalingam,  
636 S., Princevac, M., and Jung, H.: Particle size distributions from laboratory-scale biomass fires  
637 using fast response instruments, *Atmos. Chem. Phys.*, 10, 8065-8076, [https://doi.org/10.5194/acp-](https://doi.org/10.5194/acp-10-8065-2010)  
638 [10-8065-2010](https://doi.org/10.5194/acp-10-8065-2010), 2010.
- 639 Jacobson, M. Z.: Strong radiative heating due to the mixing state of black carbon in atmospheric  
640 aerosols, *Nature*, 409, 695-697, <https://doi.org/10.1038/35055518>, 2001.
- 641 Jen, C. N., Hatch, L. E., Selimovic, V., Yokelson, R. J., Weber, R., Fernandez, A. E., Kreisberg,  
642 N. M., Barsanti, K. C., and Goldstein, A. H.: Speciated and total emission factors of particulate  
643 organics from burning western U.S. wildland fuels and their dependence on combustion efficiency,  
644 *Atmos. Chem. Phys.*, 19, 1013-1026, <https://doi.org/10.5194/acp-19-1013-2019>, 2019.
- 645 Kiendler-Scharr, A., Mensah, A. A., Friese, E., Topping, D., Nemitz, E., Prevot, A. S. H., Äijälä,  
646 M., Allan, J., Canonaco, F., Canagaratna, M., Carbone, S., Crippa, M., Dall'Osto, M., Day, D. A.,  
647 De Carlo, P., Di Marco, C. F., Elbern, H., Eriksson, A., Freney, E., Hao, L., Herrmann, H.,



- 648 Hildebrandt, L., Hillamo, R., Jimenez, J. L., Laaksonen, A., McFiggans, G., Mohr, C., O'Dowd,  
649 C., Otjes, R., Ovadnevaite, J., Pandis, S. N., Poulain, L., Schlag, P., Sellegri, K., Swietlicki, E.,  
650 Tiitta, P., Vermeulen, A., Wahner, A., Worsnop, D., and Wu, H.-C.: Ubiquity of organic nitrates  
651 from nighttime chemistry in the European submicron aerosol, *Geophysical Research Letters*, 43,  
652 7735-7744, <https://doi.org/doi:10.1002/2016GL069239>, 2016.
- 653 Kirchstetter, T. W., Novakov, T., and Hobbs, P. V.: Evidence that the spectral dependence of light  
654 absorption by aerosols is affected by organic carbon, *Journal of Geophysical Research-*  
655 *Atmospheres*, 109, D21208, 2004.
- 656 Kondo, Y., Matsui, H., Moteki, N., Sahu, L., Takegawa, N., Kajino, M., Zhao, Y., Cubison, M. J.,  
657 Jimenez, J. L., Vay, S., Diskin, G. S., Anderson, B., Wisthaler, A., Mikoviny, T., Fuelberg, H. E.,  
658 Blake, D. R., Huey, G., Weinheimer, A. J., Knapp, D. J., and Brune, W. H.: Emissions of black  
659 carbon, organic, and inorganic aerosols from biomass burning in North America and Asia in 2008,  
660 *J. Geophys. Res.*, 116, D08204, <https://doi.org/10.1029/2010jd015152>, 2011.
- 661 Koss, A. R., Sekimoto, K., Gilman, J. B., Selimovic, V., Coggon, M. M., Zarzana, K. J., Yuan, B.,  
662 Lerner, B. M., Brown, S. S., Jimenez, J. L., Krechmer, J., Roberts, J. M., Warneke, C., Yokelson,  
663 R. J., and de Gouw, J.: Non-methane organic gas emissions from biomass burning: identification,  
664 quantification, and emission factors from PTR-ToF during the FIREX 2016 laboratory experiment,  
665 *Atmos. Chem. Phys.*, 18, 3299-3319, <https://doi.org/10.5194/acp-18-3299-2018>, 2018.
- 666 Lack, D. A., Cappa, C. D., Cross, E. S., Massoli, P., Ahern, A. T., Davidovits, P., and Onasch, T.  
667 B.: Absorption Enhancement of Coated Absorbing Aerosols: Validation of the Photo-Acoustic  
668 Technique for Measuring the Enhancement, *Aerosol Science and Technology*, 43, 1006-1012,  
669 <https://doi.org/10.1080/02786820903117932>, 2009.
- 670 Lack, D. A., Langridge, J., Bahreini, R., Cappa, C. D., Middlebrook, A., and Schwarz, J. P.: Brown  
671 Carbon and Internal Mixing in Biomass Burning Particles, *PNAS*, 10, 14802-14807,  
672 <https://doi.org/10.1073/pnas.1206575109>, 2012a.
- 673 Lack, D. A., Richardson, M. S., Law, D., Langridge, J. M., Cappa, C. D., McLaughlin, R. J., and  
674 Murphy, D. M.: Aircraft Instrument for Comprehensive Characterization of Aerosol Optical  
675 Properties, Part 2: Black and Brown Carbon Absorption and Absorption Enhancement Measured  
676 with Photo Acoustic Spectroscopy, *Aerosol Science and Technology*, 46, 555-568,  
677 <https://doi.org/10.1080/02786826.2011.645955>, 2012b.
- 678 Lack, D. A., Bahreini, R., Langridge, J. M., Gilman, J. B., and Middlebrook, A. M.: Brown carbon  
679 absorption linked to organic mass tracers in biomass burning particles, *Atmos. Chem. Phys.*, 13,  
680 2415-2422, <https://doi.org/10.5194/acp-13-2415-2013>, 2013.
- 681 Langridge, J. M., Richardson, M. S., Lack, D., Law, D., and Murphy, D. M.: Aircraft Instrument  
682 for Comprehensive Characterization of Aerosol Optical Properties, Part I: Wavelength-Dependent  
683 Optical Extinction and Its Relative Humidity Dependence Measured Using Cavity Ringdown  
684 Spectroscopy, *Aerosol Science and Technology*, 45, 1305-1318,  
685 <https://doi.org/10.1080/02786826.2011.592745>, 2011.
- 686 Laskin, A., Lin, P., Laskin, J., Fleming, L. T., and Nizkorodov, S.: Molecular Characterization of  
687 Atmospheric Brown Carbon, in: *Multiphase Environmental Chemistry in the Atmosphere*, ACS  
688 Symposium Series, 1299, American Chemical Society, 261-274, 2018.



- 689 Levin, E. J. T., McMeeking, G. R., Carrico, C. M., Mack, L. E., Kreidenweis, S. M., Wold, C. E.,  
690 Moosmüller, H., Arnott, W. P., Hao, W. M., Collett, J. L., and Malm, W. C.: Biomass burning  
691 smoke aerosol properties measured during Fire Laboratory at Missoula Experiments (FLAME),  
692 Journal of Geophysical Research: Atmospheres, 115, D18210,  
693 <https://doi.org/10.1029/2009JD013601>, 2010.
- 694 Lim, C. Y., Hagan, D. H., Coggon, M. M., Koss, A. R., Sekimoto, K., De Gouw, J., Warneke, C.,  
695 Cappa, C. D., and Kroll, J. H.: Secondary organic aerosol formation from biomass burning  
696 emissions, Atmos. Chem. Phys. Discuss., <https://doi.org/10.5194/acp-2019-326>, 2019.
- 697 Lin, P., Aiona, P. K., Li, Y., Shiraiwa, M., Laskin, J., Nizkorodov, S. A., and Laskin, A.: Molecular  
698 Characterization of Brown Carbon in Biomass Burning Aerosol Particles, Environmental Science  
699 & Technology, 50, 11815-11824, <https://doi.org/10.1021/acs.est.6b03024>, 2016.
- 700 Liu, D. T., Whitehead, J., Alfarra, M. R., Reyes-Villegas, E., Spracklen, D. V., Reddington, C. L.,  
701 Kong, S. F., Williams, P. I., Ting, Y. C., Haslett, S., Taylor, J. W., Flynn, M. J., Morgan, W. T.,  
702 McFiggans, G., Coe, H., and Allan, J. D.: Black-carbon absorption enhancement in the atmosphere  
703 determined by particle mixing state, Nat. Geosci., 10, 184-U132,  
704 <https://doi.org/10.1038/ngeo2901>, 2017.
- 705 Liu, S., Aiken, A. C., Arata, C., Dubey, M. K., Stockwell, C. E., Yokelson, R. J., Stone, E. A.,  
706 Jayarathne, T., Robinson, A. L., DeMott, P. J., and Kreidenweis, S. M.: Aerosol single scattering  
707 albedo dependence on biomass combustion efficiency: Laboratory and field studies, Geophysical  
708 Research Letters, 2013GL058392, <https://doi.org/10.1002/2013GL058392>, 2013.
- 709 Liu, S., Aiken, A. C., Gorkowski, K., Dubey, M. K., Cappa, C. D., Williams, L. R., Herndon, S.  
710 C., Massoli, P., Fortner, E. C., Chhabra, P. S., Brooks, W. A., Onasch, T. B., Worsnop, D. R.,  
711 China, S., Sharma, N., Mazzoleni, C., Xu, L., L., N. N., Liu, D., Allan, J. D., Lee, J. D., Fleming,  
712 Z. L., Mohr, C., Zotter, P., Szidat, S., and Prevot, A. S. H.: Enhanced light absorption by mixed  
713 source black and brown carbon particles in UK winter, Nat. Comm., 6, 8435,  
714 <https://doi.org/10.1038/ncomms9435>, 2015.
- 715 Mann, G. W., Carslaw, K. S., Reddington, C. L., Pringle, K. J., Schulz, M., Asmi, A., Spracklen,  
716 D. V., Ridley, D. A., Woodhouse, M. T., Lee, L. A., Zhang, K., Ghan, S. J., Easter, R. C., Liu, X.,  
717 Stier, P., Lee, Y. H., Adams, P. J., Tost, H., Lelieveld, J., Bauer, S. E., Tsigaridis, K., van Noije,  
718 T. P. C., Strunk, A., Vignati, E., Bellouin, N., Dalvi, M., Johnson, C. E., Bergman, T., Kokkola,  
719 H., von Salzen, K., Yu, F., Luo, G., Petzold, A., Heintzenberg, J., Clarke, A., Ogren, J. A., Gras,  
720 J., Baltensperger, U., Kaminski, U., Jennings, S. G., O'Dowd, C. D., Harrison, R. M., Beddows,  
721 D. C. S., Kulmala, M., Viisanen, Y., Ulevicius, V., Mihalopoulos, N., Zdimal, V., Fiebig, M.,  
722 Hansson, H. C., Swietlicki, E., and Henzing, J. S.: Intercomparison and evaluation of global  
723 aerosol microphysical properties among AeroCom models of a range of complexity, Atmos. Chem.  
724 Phys., 14, 4679-4713, <https://doi.org/10.5194/acp-14-4679-2014>, 2014.
- 725 May, A. A., McMeeking, G. R., Lee, T., Taylor, J. W., Craven, J. S., Burling, I., Sullivan, A. P.,  
726 Akagi, S., Collett Jr., J. L., Flynn, M., Coe, H., Urbanski, S. P., Seinfeld, J. H., Yokelson, R. J.,  
727 and Kreidenweis, S. M.: Aerosol emissions from prescribed fires in the United States: A synthesis  
728 of laboratory and aircraft measurements, Journal of Geophysical Research: Atmospheres, 119,  
729 11,826-811,849, <https://doi.org/10.1002/2014JD021848>, 2014.
- 730 McMeeking, G. R., Kreidenweis, S. M., Baker, S., Carrico, C. M., Chow, J. C., Collett, J. L., Hao,  
731 W. M., Holden, A. S., Kirchstetter, T. W., Malm, W. C., Moosmüller, H., Sullivan, A. P., and



- 732 Wold, C. E.: Emissions of trace gases and aerosols during the open combustion of biomass in the  
733 laboratory, *Journal of Geophysical Research: Atmospheres*, 114, D19210,  
734 <https://doi.org/10.1029/2009JD011836>, 2009.
- 735 McMeeking, G. R., Fortner, E., Onasch, T. B., Taylor, J. W., Flynn, M., Coe, H., and Kreidenweis,  
736 S. M.: Impacts of nonrefractory material on light absorption by aerosols emitted from biomass  
737 burning, *Journal of Geophysical Research: Atmospheres*, 119, 12,272-212,286,  
738 <https://doi.org/10.1002/2014JD021750>, 2014.
- 739 Metcalf, A. R., Loza, C. L., Coggon, M. M., Craven, J. S., Jonsson, H. H., Flagan, R. C., and  
740 Seinfeld, J. H.: Secondary Organic Aerosol Coating Formation and Evaporation: Chamber Studies  
741 Using Black Carbon Seed Aerosol and the Single-Particle Soot Photometer, *Aerosol Sci. Technol.*,  
742 47, 326-347, <https://doi.org/10.1080/02786826.2012.750712>, 2013.
- 743 Mohr, C., Lopez-Hilfiker, F. D., Zotter, P., Prévôt, A. S. H., Xu, L., Ng, N. L., Herndon, S. C.,  
744 Williams, L. R., Franklin, J. P., Zahniser, M. S., Worsnop, D. R., Knighton, W. B., Aiken, A. C.,  
745 Gorkowski, K. J., Dubey, M. K., Allan, J. D., and Thornton, J. A.: Contribution of Nitrated Phenols  
746 to Wood Burning Brown Carbon Light Absorption in Detling, United Kingdom during Winter  
747 Time, *Environmental Science & Technology*, 47, 6316-6324, <https://doi.org/10.1021/es400683v>,  
748 2013.
- 749 Onasch, T. B., Trimborn, A. M., Fortner, E. C., Jayne, J. T., Kok, G. L., Williams, L. R.,  
750 Davidovits, P., and Worsnop, D. R.: Soot Particle Aerosol Mass Spectrometer: Development,  
751 Validation and Initial Application, *Aerosol Science and Technology*, 46, 804-817,  
752 <https://doi.org/10.1080/02786826.2012.663948>, 2012.
- 753 Peng, J., Hu, M., Guo, S., Du, Z., Zheng, J., Shang, D., Zamora, M. L., Zeng, L., Shao, M., Wu,  
754 Y.-S., Zheng, J., Wang, Y., Glen, C. R., Collins, D. R., Molina, M. J., and Zhang, R.: Markedly  
755 enhanced absorption and direct radiative forcing of black carbon under polluted urban  
756 environments, *Proc. Natl. Acad. Sci. U. S. A.*, 113, 4266-4271,  
757 <https://doi.org/10.1073/pnas.1602310113>, 2016.
- 758 Pokhrel, R. P., Wagner, N. L., Langridge, J. M., Lack, D. A., Jayarathne, T., Stone, E. A.,  
759 Stockwell, C. E., Yokelson, R. J., and Murphy, S. M.: Parameterization of single-scattering albedo  
760 (SSA) and absorption Ångström exponent (AAE) with EC/OC for aerosol emissions from  
761 biomass burning, *Atmos. Chem. Phys.*, 16, 9549-9561, <https://doi.org/10.5194/acp-16-9549-2016>,  
762 2016.
- 763 Pokhrel, R. P., Beamesderfer, E. R., Wagner, N. L., Langridge, J. M., Lack, D. A., Jayarathne, T.,  
764 Stone, E. A., Stockwell, C. E., Yokelson, R. J., and Murphy, S. M.: Relative importance of black  
765 carbon, brown carbon, and absorption enhancement from clear coatings in biomass burning  
766 emissions, *Atmospheric Chemistry and Physics*, 17, 5063-5078, [https://doi.org/10.5194/acp-17-  
767 5063-2017](https://doi.org/10.5194/acp-17-5063-2017), 2017.
- 768 Qin, Y. M., Tan, H. B., Li, Y. J., Li, Z. J., Schurman, M. I., Liu, L., Wu, C., and Chan, C. K.:  
769 Chemical characteristics of brown carbon in atmospheric particles at a suburban site near  
770 Guangzhou, China, *Atmos. Chem. Phys.*, 18, 16409-16418, [https://doi.org/10.5194/acp-18-16409-  
771 2018](https://doi.org/10.5194/acp-18-16409-2018), 2018.
- 772 Reid, J. S., Koppmann, R., Eck, T. F., and Eleuterio, D. P.: A review of biomass burning emissions  
773 part II: intensive physical properties of biomass burning particles, *Atmos. Chem. Phys.*, 5, 799-  
774 825, <https://doi.org/10.5194/acp-5-799-2005>, 2005.



- 775 Sahu, L. K., Kondo, Y., Moteki, N., Takegawa, N., Zhao, Y., Cubison, M. J., Jimenez, J. L., Vay,  
776 S., Diskin, G. S., Wisthaler, A., Mikoviny, T., Huey, L. G., Weinheimer, A. J., and Knapp, D. J.:  
777 Emission characteristics of black carbon in anthropogenic and biomass burning plumes over  
778 California during ARCTAS-CARB 2008, *Journal of Geophysical Research-Atmospheres*, 117,  
779 <https://doi.org/10.1029/2011jd017401>, 2012.
- 780 Saleh, R., Hennigan, C. J., McMeeking, G. R., Chuang, W. K., Robinson, E. S., Coe, H., Donahue,  
781 N. M., and Robinson, A. L.: Absorptivity of brown carbon in fresh and photo-chemically aged  
782 biomass-burning emissions, *Atmospheric Chemistry and Physics*, 13, 7683-7693,  
783 <https://doi.org/10.5194/acp-13-7683-2013>, 2013.
- 784 Saleh, R., Robinson, E. S., Tkacik, D. S., Ahern, A. T., Liu, S., Aiken, A. C., Sullivan, R. C.,  
785 Presto, A. A., Dubey, M. K., Yokelson, R. J., Donahue, N. M., and Robinson, A. L.: Brownness  
786 of organics in aerosols from biomass burning linked to their black carbon content, *Nature Geosci*,  
787 7, 647-650, <https://doi.org/10.1038/ngeo2220>, 2014.
- 788 Saleh, R., Cheng, Z., and Atwi, K.: The Brown-Black Continuum of Light-Absorbing Combustion  
789 Aerosols, *Environmental Science & Technology Letters*, ASAP,  
790 <https://doi.org/10.1021/acs.estlett.8b00305>, 2018.
- 791 Schneider, J., Weimer, S., Drewnick, F., Borrmann, S., Helas, G., Gwaze, P., Schmid, O., Andreae,  
792 M. O., and Kirchner, U.: Mass spectrometric analysis and aerodynamic properties of various types  
793 of combustion-related aerosol particles, *International Journal of Mass Spectrometry*, 258, 37-49,  
794 <https://doi.org/10.1016/j.ijms.2006.07.008>, 2006.
- 795 Schwarz, J. P., Gao, R. S., Spackman, J. R., Watts, L. A., Thomson, D. S., Fahey, D. W., Ryerson,  
796 T. B., Peischl, J., Holloway, J. S., Trainer, M., Frost, G. J., Baynard, T., Lack, D. A., de Gouw, J.  
797 A., Warneke, C., and Del Negro, L. A.: Measurement of the mixing state, mass, and optical size  
798 of individual black carbon particles in urban and biomass burning emissions, *Geophysical*  
799 *Research Letters*, 35, L13810, <https://doi.org/10.1029/2008gl033968>, 2008.
- 800 Sekimoto, K., Koss, A. R., Gilman, J. B., Selimovic, V., Coggon, M. M., Zarzana, K. J., Yuan, B.,  
801 Lerner, B. M., Brown, S. S., Warneke, C., Yokelson, R. J., Roberts, J. M., and de Gouw, J.: High-  
802 and low-temperature pyrolysis profiles describe volatile organic compound emissions from  
803 western US wildfire fuels, *Atmos. Chem. Phys.*, 18, 9263-9281, [https://doi.org/10.5194/acp-18-](https://doi.org/10.5194/acp-18-9263-2018)  
804 [9263-2018](https://doi.org/10.5194/acp-18-9263-2018), 2018.
- 805 Shamjad, P. M., Tripathi, S. N., Thamban, N. M., and Vreeland, H.: Refractive Index and  
806 Absorption Attribution of Highly Absorbing Brown Carbon Aerosols from an Urban Indian City-  
807 Kanpur, *Scientific Reports*, 6, 37735, <https://doi.org/10.1038/srep37735>, 2016.
- 808 Shiraiwa, M., Kondo, Y., Iwamoto, T., and Kita, K.: Amplification of Light Absorption of Black  
809 Carbon by Organic Coating, *Aerosol Science and Technology*, 44, 46-54,  
810 <https://doi.org/10.1080/02786820903357686>, 2010.
- 811 Sumlin, B. J., Pandey, A., Walker, M. J., Pattison, R. S., Williams, B. J., and Chakrabarty, R. K.:  
812 Atmospheric Photooxidation Diminishes Light Absorption by Primary Brown Carbon Aerosol  
813 from Biomass Burning, *Environmental Science & Technology Letters*, 4, 540-545,  
814 <https://doi.org/10.1021/acs.estlett.7b00393>, 2017.
- 815 Wandinger, Ulla, Müller, Detlef, Böckmann, Christine, Althausen, Dietrich, Matthias, Volker,  
816 Bösenberg, Jens, Weiß, Volker, Fiebig, Markus, Wendisch, Manfred, Stohl, Andreas, and



- 817 Ansmann, A.: Optical and microphysical characterization of biomass- burning and industrial-  
818 pollution aerosols from- multiwavelength lidar and aircraft measurements, *Journal of Geophysical*  
819 *Research: Atmospheres*, 107, LAC 7-1-LAC 7-20, <https://doi.org/doi:10.1029/2000JD000202>,  
820 2002.
- 821 Washenfelder, R. A., Attwood, A. R., Brock, C. A., Guo, H., Xu, L., Weber, R. J., Ng, N. L., Allen,  
822 H. M., Ayres, B. R., Baumann, K., Cohen, R. C., Draper, D. C., Duffey, K. C., Edgerton, E., Fry,  
823 J. L., Hu, W. W., Jimenez, J. L., Palm, B. B., Romer, P., Stone, E. A., Wooldridge, P. J., and  
824 Brown, S. S.: Biomass burning dominates brown carbon absorption in the rural southeastern  
825 United States, *Geophysical Research Letters*, 42, 653-664,  
826 <https://doi.org/10.1002/2014GL062444>, 2015.
- 827 Xie, M., Hays, M. D., and Holder, A. L.: Light-absorbing organic carbon from prescribed and  
828 laboratory biomass burning and gasoline vehicle emissions, *Scientific Reports*, 7, 7318,  
829 <https://doi.org/10.1038/s41598-017-06981-8>, 2017.
- 830 Yang, M., Howell, S. G., Zhuang, J., and Huebert, B. J.: Attribution of aerosol light absorption to  
831 black carbon, brown carbon, and dust in China – interpretations of atmospheric measurements  
832 during EAST-AIRE, *Atmospheric Chemistry and Physics*, 9, 2035-2050,  
833 <https://doi.org/10.5194/acp-9-2035-2009>, 2009.
- 834 Zhang, X., Kim, H., Parworth, C., Young, D. E., Zhang, Q., Metcalf, A. R., and Cappa, C. D.:  
835 Optical Properties of Wintertime Aerosols from Residential Wood Burning in Fresno, CA: Results  
836 from DISCOVER-AQ 2013, *Environmental Science & Technology*, 50, 1681-1690,  
837 <https://doi.org/10.1021/acs.est.5b04134>, 2016.
- 838
- 839



840

841 **9 Tables**

842 **Table 1.** Fuels by particle Class.

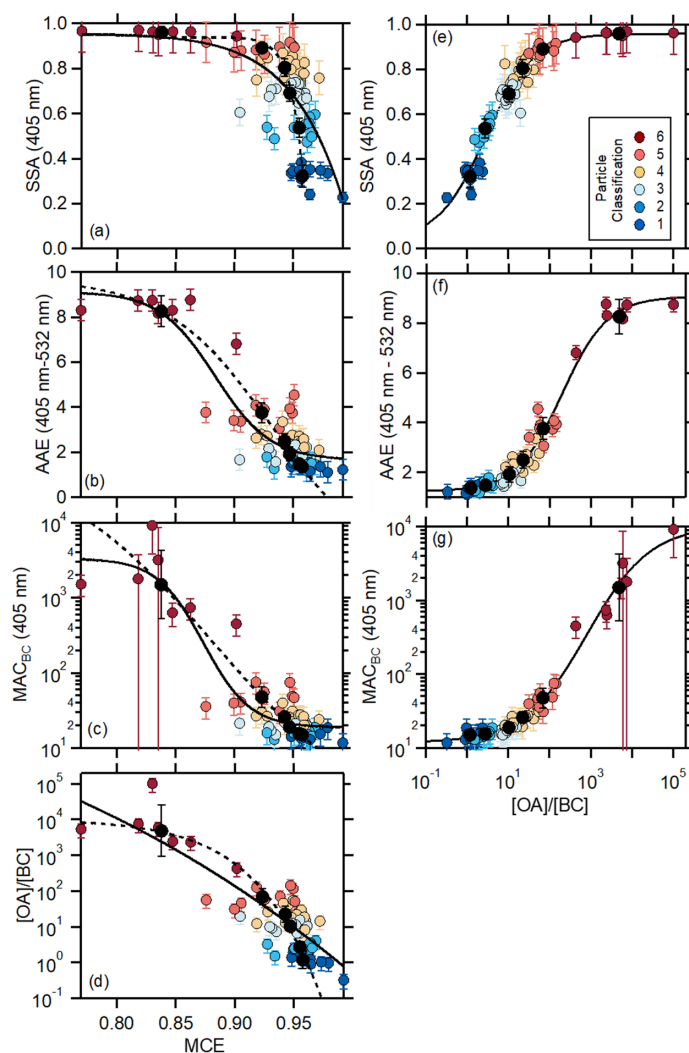
Class	Fuel	SSA range	[OA]/[BC] range
Class 1	Chaparral, canopy, litter (pine), building materials, excelsior	0.23-0.43	0.3-2.4
Class 2	Manzanita, Sage, litter (fir)	0.43-0.60	1.5-4.1
Type 3	Pine, fir, litter, canopy, juniper	0.60-0.74	6.6-20
Class 4	Pine, fir, canopy, rotten log, ceonothos	0.74-0.87	8.3-55
Class 5	Canopy (pine), rice, bear grass, duff	0.87-0.93	31-143
Class 6	Rotten log, duff, peat, dung	0.93-1.00	431-10 <sup>5</sup>

843

844



845 **10 Figures**

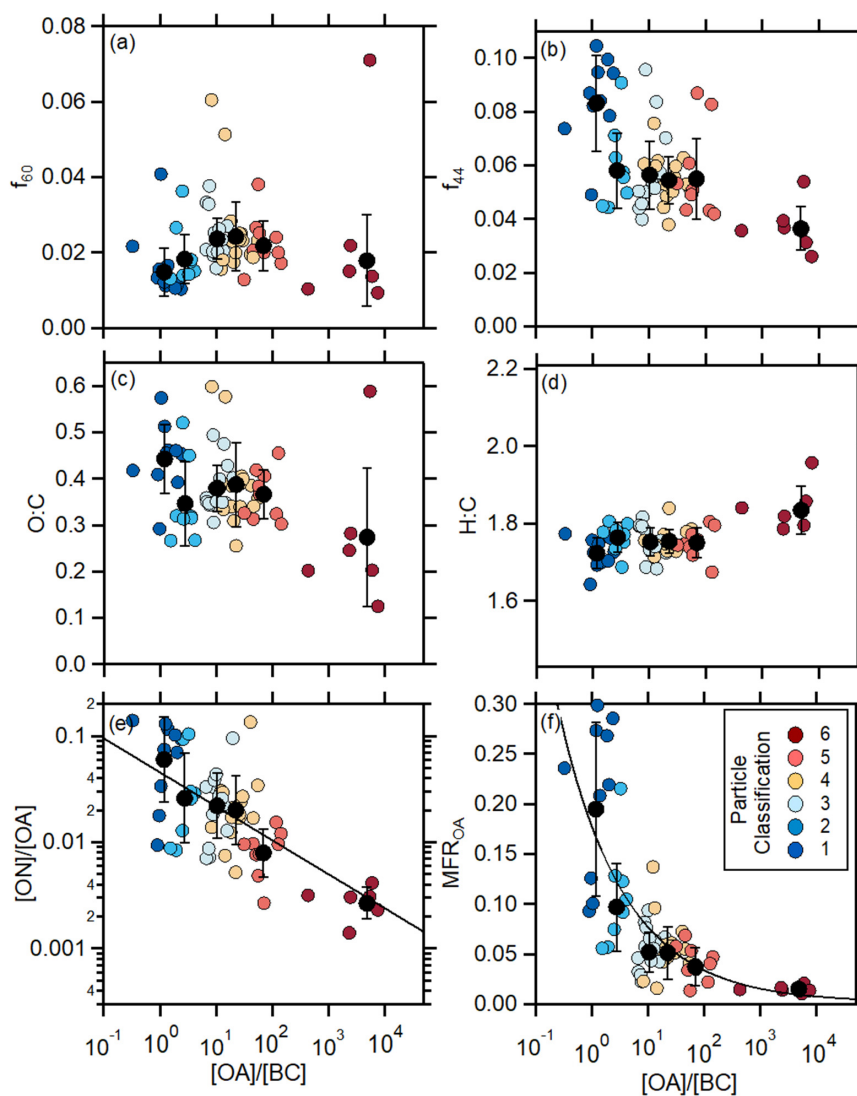


846

847 **Figure 1.** (left panels) Relationship between (a) the  $SSA_{405nm}$ , (b) the  $AAE_{405-532}$ , (c) the  $MAC_{BC}$ ,  
848 and (d) the  $[OA]/[BC]$  mass ratio and the modified combustion efficiency, MCE. Results for  
849 individual burns are shown as points colored by the particle Class, and Class average values are  
850 shown as black circles. Uncertainties on the Class averages are  $1\sigma$  based on measurement  
851 variability and uncertainties on for the individual burns are from error propagation of measurement  
852 uncertainties. The solid black lines are fits to the individual burns (colored points) while the dashed  
853 black lines are fits to the Class averages (Table S2). (right panels) Relationship between (e) the  
854  $SSA_{405nm}$ , (f) the  $AAE_{405-532}$ , and (g) the  $MAC_{BC}$  on the  $[OA]/[BC]$  mass ratio. The solid black  
855 lines here are sigmoidal fits to the individual burns. Fits to the Class averages are similar.



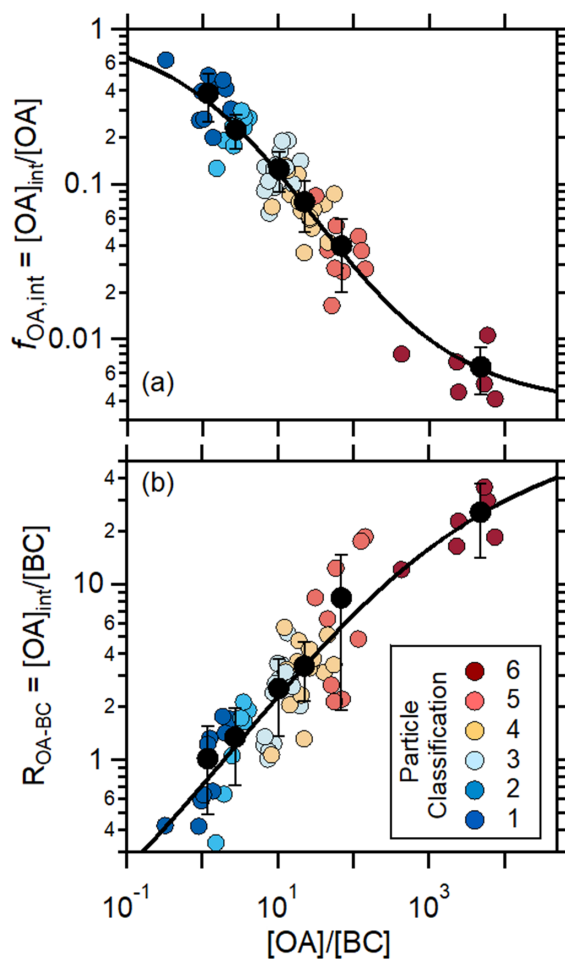
856



857

858 **Figure 2.** Dependence of (a)  $f_{60}$ , (b)  $f_{44}$ , (c) O:C, (d) H:C, (e) the nitrated organic fraction of OA,  
859  $f_{\text{ON-OA}}$ , and (f) the OA volatility, characterized as the mass fraction remaining after heating. Results  
860 for individual burns are shown as points colored by the particle Class, and Class average values  
861 are shown as black circles. Uncertainties on the Class averages are  $1\sigma$  based on measurement  
862 variability. For  $f_{\text{ON-OA}}$  and  $MFR_{\text{OA}}$ , fits to the observations are shown (see text).

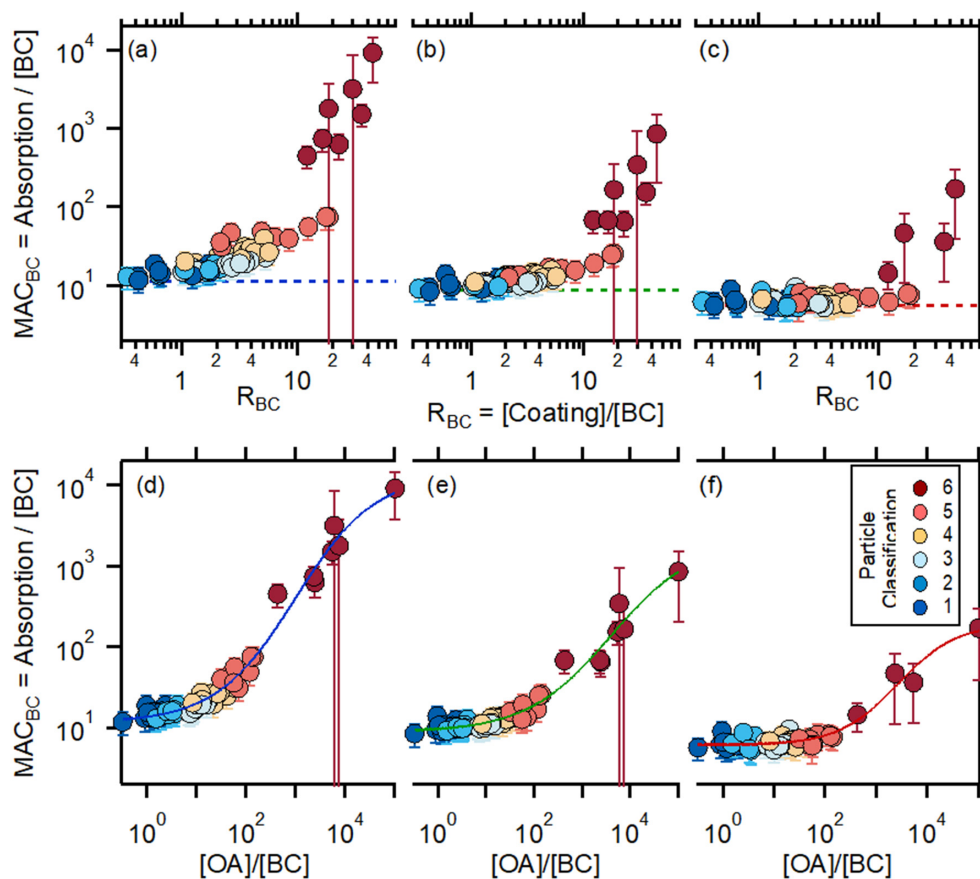
863



864

865 **Figure 3.** Relationship between (a) the fraction of OA that is internally mixed with BC,  $f_{\text{OA,int}}$  and  
866 (b) the OA-to-BC mass ratio for only the internally mixed OA, and the total  $[\text{OA}]/[\text{BC}]$  mass ratio.  
867 Results for individual burns are shown as points colored by the particle Class, and Class average  
868 values are shown as black circles. Uncertainties on the Class averages are  $1\sigma$  based on  
869 measurement variability. Black lines are sigmoidal fits to the data, in log-log space.

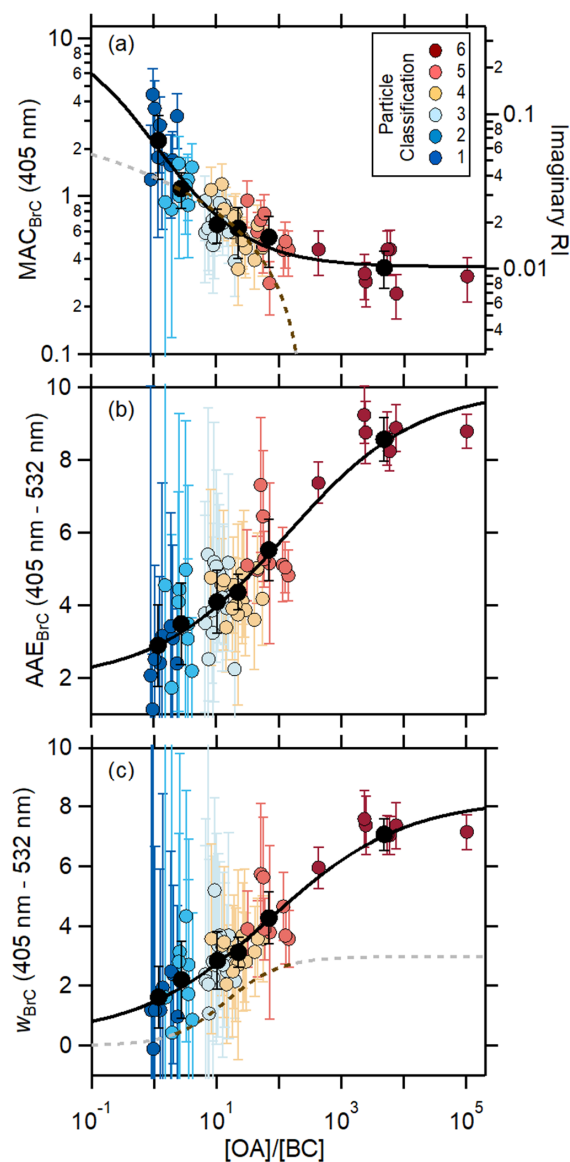
870



871

872 **Figure 4.** (Top Panels) The relationship between the wavelength-dependent  $MAC_{BC}$  and the  
873 coating-to-BC mass ratio for (a) 405 nm, (b) 532 nm and (c) 781 nm. The horizontal dashed lines  
874 show the derived  $MAC_{BC,pure}$  values. (Bottom Panels) The relationship between the wavelength-  
875 dependent  $MAC_{BC}$  and the total  $[OA]/[BC]$  mass ratio for (a) 405 nm, (b) 532 nm and (c) 781 nm.  
876 The lines are sigmoidal fits. Uncertainties for the individual burns are determined from error  
877 propagation.

878

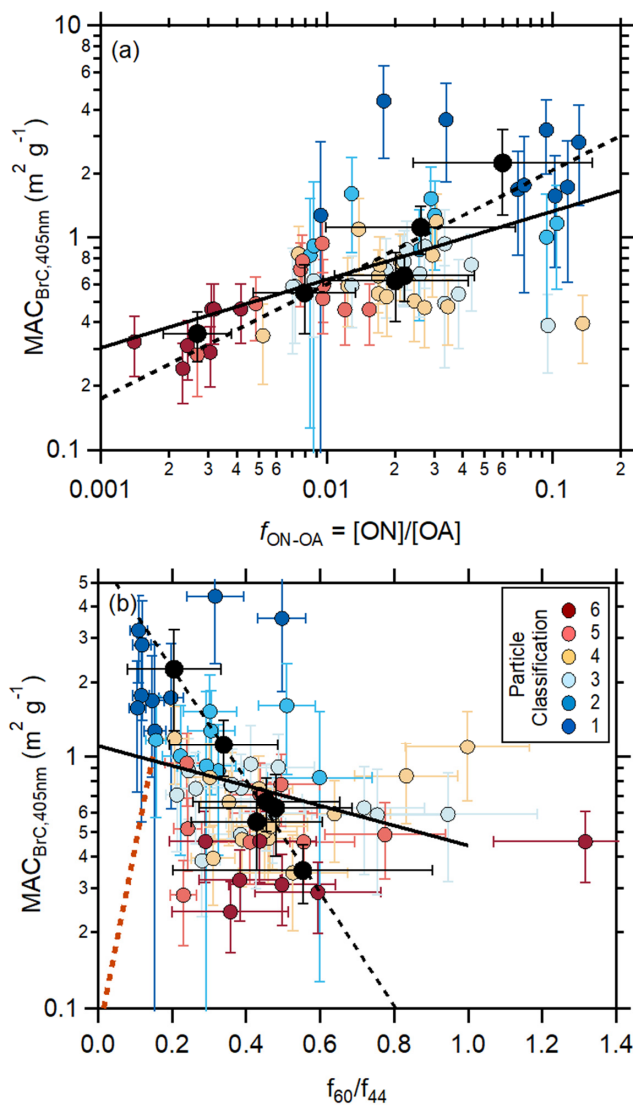


879

880 **Figure 5.** Relationship between (a)  $MAC_{BrC,405nm}$ , (b)  $AAE_{BrC,405-532}$ , and (c)  $W_{BrC,405-532}$  and the  
881  $[OA]/[BC]$  mass ratio. The solid lines are sigmoidal fits to the observations, against  
882  $\log([OA]/[BC])$ . The dashed lines are based on the parameterization of Saleh et al. (2014), with  
883 the brown color indicating the measuring range in that study and the gray color extrapolated.  
884 Results for individual burns are shown as points colored by the particle Class, and Class average  
885 values are shown as black circles. Uncertainties on the Class averages are  $1\sigma$  based on  
886 measurement variability. Uncertainties for the individual burns are determined from error  
887 propagation.



888

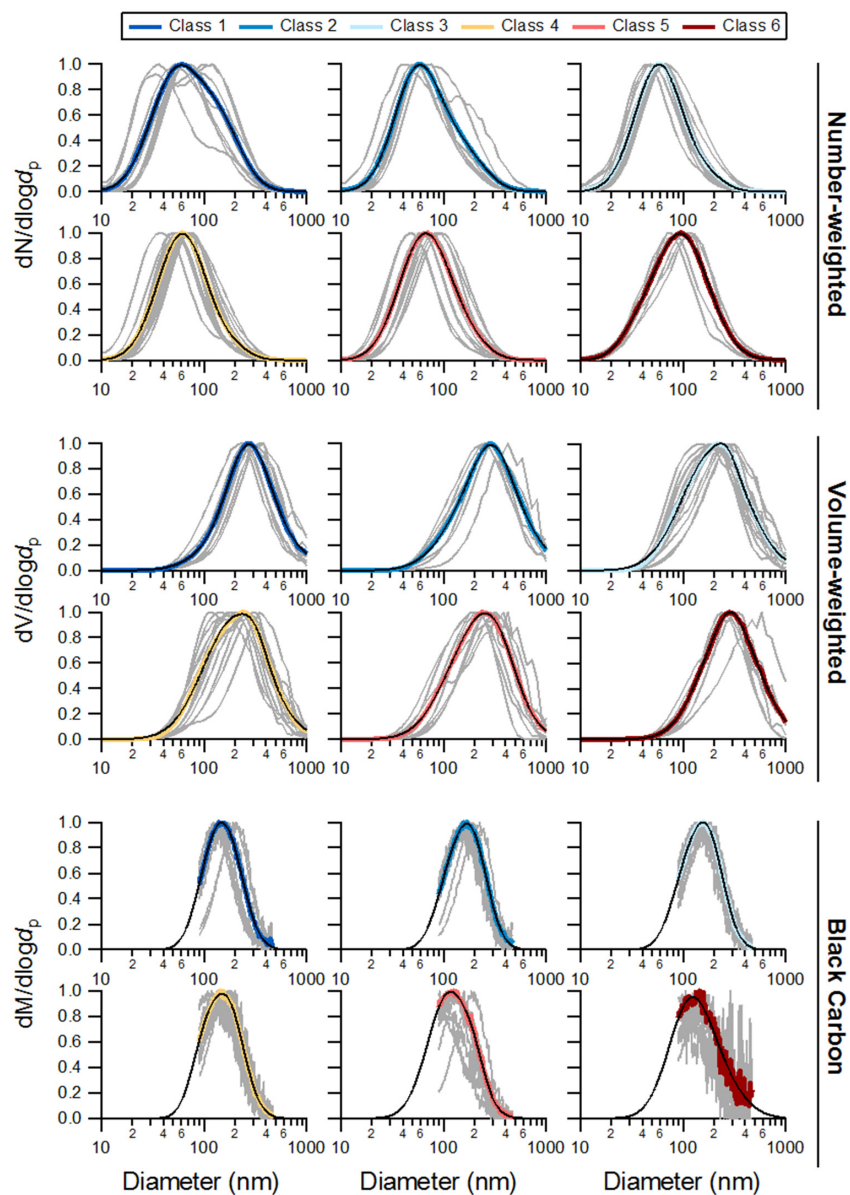


889

890 **Figure 6.** Relationship between the  $MAC_{BrC,405nm}$  and (a) the nitrated organic fraction of total  
891 organic aerosol,  $f_{ON-OA}$ , and (b) the  $f_{60}/f_{44}$  ion ratio for organic aerosol. Results for individual burns  
892 are shown as points colored by the particle Class, and Class average values are shown as black  
893 circles. Uncertainties on the Class averages are  $1\sigma$  based on measurement variability. Uncertainties  
894 for the individual burns are determined from error propagation. Solid black lines are fits to all  
895 burns and dashed black lines are fits to the Class averages. The dashed brown line in panel (b) is  
896 the relationship reported by Lack et al. (2013) for ambient particles in a biomass burning plume.

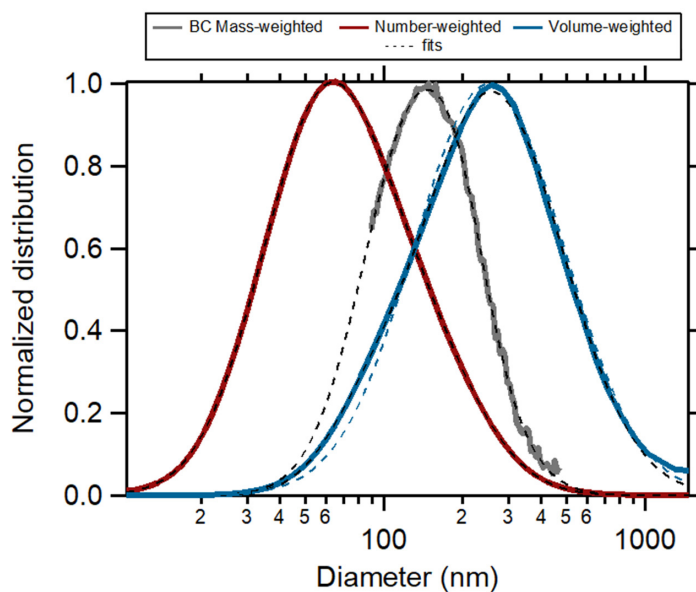


897



898

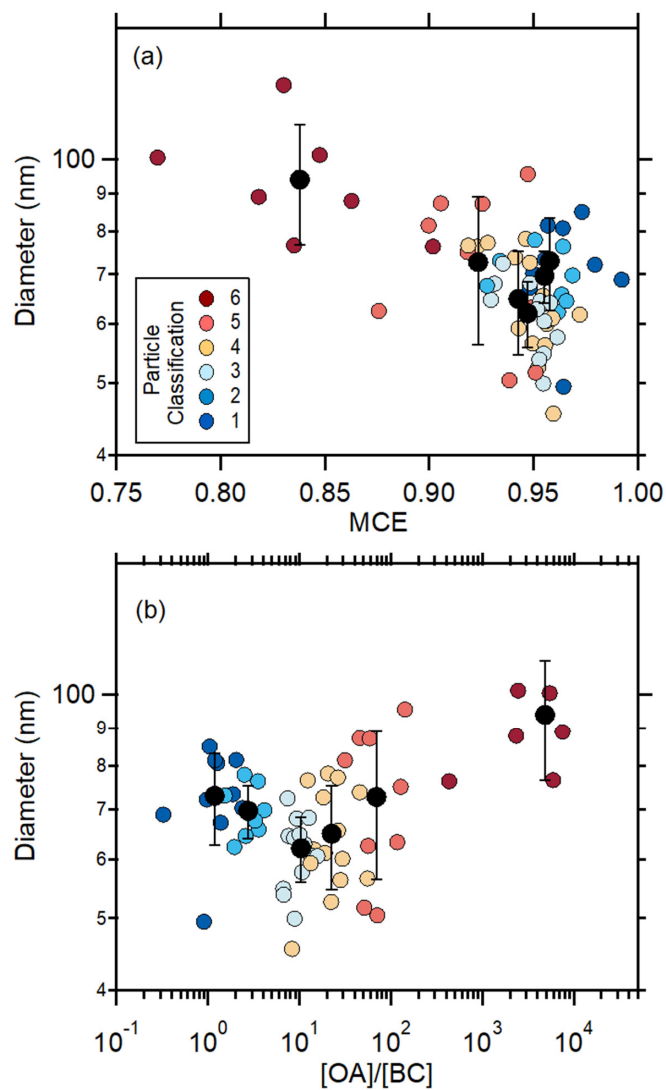
899 **Figure 7.** Class-specific total particle number-weighted (top) and volume-weighted (middle)  
900 mobility size distributions, and the BC-only mass-weighted (bottom) size distribution. Individual  
901 burns are shown in gray and class averages are shown as colors. Bimodal log-normal fits are thin  
902 black lines. Note that the number-weighted and volume-weighted distributions are graphed versus  
903 mobility diameter and the BC mass-weighted distribution against the BC volume equivalent  
904 diameter.



905

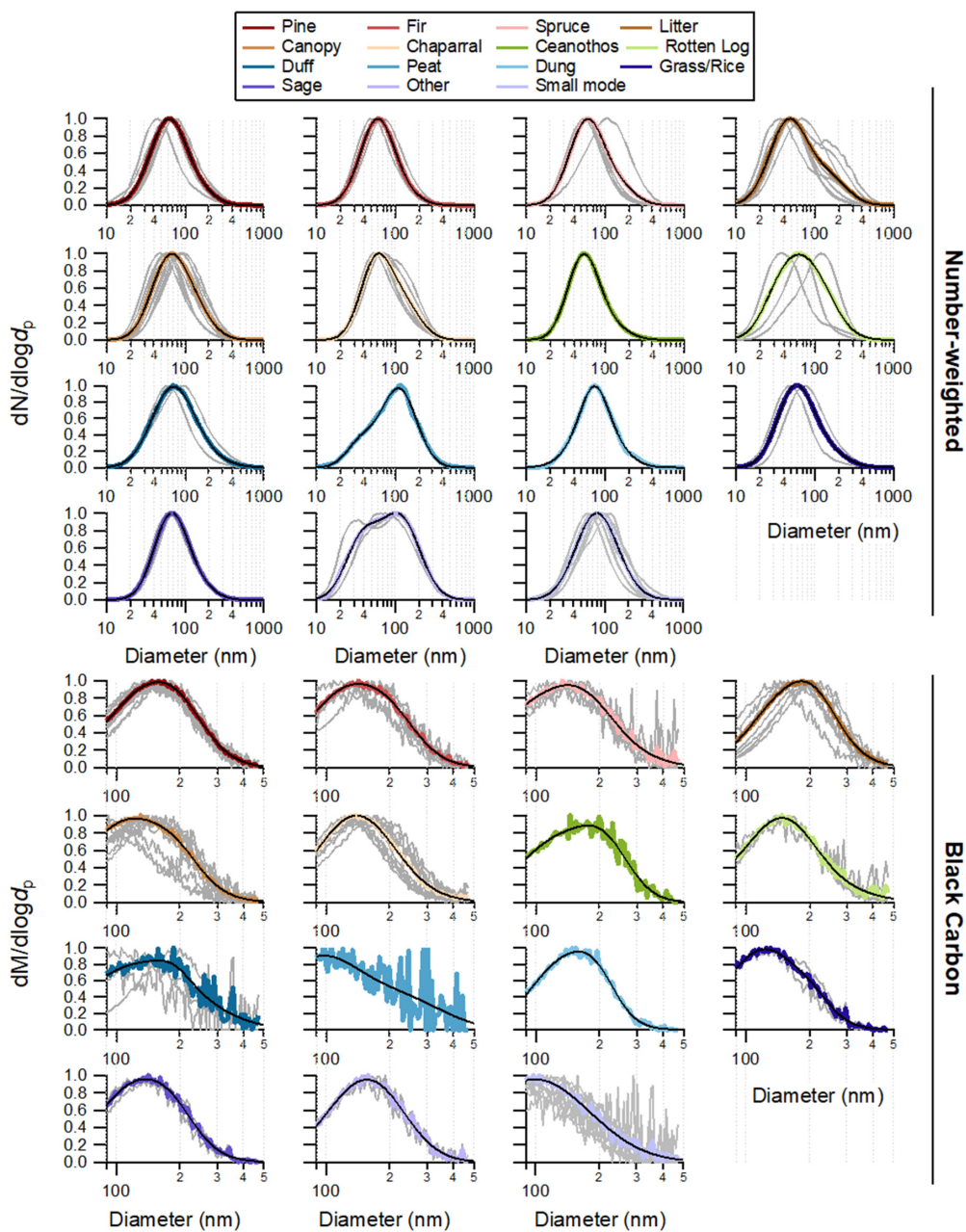
906 **Figure 8.** Average total particle number-weighted (red) and volume-weighted (blue) size  
907 distributions and the BC-specific mass-weighted size distributions. Black dashed lines are bimodal  
908 log-normal fits. The dashed blue line is the total particle volume-weighted distribution calculated  
909 from a single-mode fit to the number-weighted distribution. Note that the number-weighted and  
910 volume-weighted distributions are graphed versus mobility diameter and the BC mass-weighted  
911 distribution against the BC volume equivalent diameter.

912



913

914 **Figure 9.** Relationship between number-weighted particle median diameter and (a) the MCE and  
915 (b) the [OA]/[BC] ratio. Colored circles are for individual burns and black circles for particle class  
916 averages.



917

918 **Figure 10.** Normalized total particle number-weighted (top) and the BC-only mass-weighted  
 919 (bottom) size distributions shown by fuel type (see legend). Individual burns are gray and averages  
 920 for a fuel type colors. For some fuels there is only one size distribution. Bimodal log-normal fits  
 921 are the black lines. The “other” category includes non-traditional biofuels, specifically building  
 922 materials and excelsior.